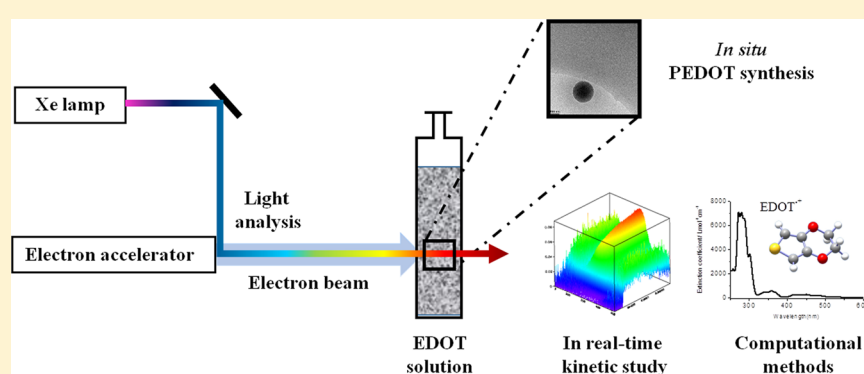


# Electron-Induced Growth Mechanism of Conducting Polymers: A Coupled Experimental and Computational Investigation

Cecilia Coletta,<sup>†</sup> Zhenpeng Cui,<sup>†</sup> Pierre Archirel,<sup>†</sup> Pascal Pernot,<sup>†</sup> Jean-Louis Marignier,<sup>†</sup> and Samy Remita<sup>\*,†,§</sup>

<sup>†</sup>Laboratoire de Chimie Physique, UMR 8000 CNRS/Université Paris-Sud, Faculté des Sciences d'Orsay, Bât 349, 91405 Orsay Cedex, France

<sup>§</sup>Département CASER, Ecole SITI, Conservatoire National des Art et Métiers, CNAM, 75141 Paris Cedex 03, France



**ABSTRACT:** Pulse radiolysis was used to study the mechanism of HO<sup>•</sup>-induced polymerization of poly(3,4-ethylenedioxythiophene), PEDOT, in aqueous solution. A step-by-step mechanism has been found which involves a recurrent oxidation process by HO<sup>•</sup> hydroxyl radicals produced by water radiolysis. Furthermore, the cation radical, EDOT<sup>•+</sup>, has been proposed as the promoter of the first step of polymerization. The determination of rate constants values and the attribution of transient and stable species were confirmed by molecular simulations and spectrokinetic analysis. Moreover, applying a series of electron pulses enabled *in situ* PEDOT polymerization. These polymers, which were characterized in solution or after deposition, form globular self-assembled structures with interesting conducting properties. Such a synthesis initiated for the first time by an electron accelerator gives us a glimpse of future promising industrial applications in the field of conducting polymers synthesis.

## INTRODUCTION

Poly(3,4-ethylenedioxythiophene), PEDOT, is one of the most versatile  $\pi$ -conjugated conducting polymers.<sup>1</sup> Covering a wide range of applications,<sup>2</sup> it is known for its remarkable properties<sup>3</sup> such as low redox potential,<sup>4</sup> low band gap<sup>5</sup> of 1.5–1.6 eV, high conductivity,<sup>6</sup> and good air stability.<sup>7,8</sup> Today it is one of the most important conjugated polymers used in industry in different devices including light-emitting diodes (OLEDs),<sup>9</sup> photovoltaic cells (OPVs),<sup>10,11</sup> or field-effect transistors (OFETs).<sup>12</sup>

Generally, like most of conducting polymers, PEDOT is synthesized either by chemical<sup>13,14</sup> or electrochemical polymerization,<sup>15–17</sup> both starting from oxidation of ethylenedioxythiophene, EDOT, monomers. Although these two methods lead to the synthesis of polymers with excellent optoelectronic properties, they do not allow to study the growth mechanism of conducting polymers. In the literature, a chain mechanism<sup>18</sup> is sometimes proposed to describe PEDOT polymerization, while a step-by-step mechanism<sup>6,9</sup> is usually evoked. Nevertheless, there is no experimental evidence to substantiate this. Yet, to control the structure of conducting polymers and to improve their properties, it is absolutely necessary to understand and thus to control the growth mechanism.

In a previous study,<sup>19,20</sup> our group evidenced a new strategy to synthesize PEDOT in aqueous solutions by using  $\gamma$ -ionizing radiation either under air or N<sub>2</sub>O atmosphere. This methodology allowed us to synthesize polymers under soft-conditions, at ambient temperature and pressure, and to obtain hydrophilic PEDOT polymers without any prefunctionalization of EDOT monomers. Moreover, our group indirectly demonstrated that a step-by-step mechanism is involved during PEDOT polymerization. Indeed, the yield of EDOT monomers consumption, which is strictly equal to the yield of formation of HO<sup>•</sup> oxidizing radicals, does not depend on the initial concentration of the monomers. On the other hand, the amount of oxidizing species which is needed for quantitative polymerization of PEDOT is twice that of EDOT monomers. These previous results indicate that no chain reaction should happen. Thus, polymerization should proceed through recurrent oxidation reactions: HO<sup>•</sup> oxidize monomers, then dimers, then oligomers, and so on.

Received: March 18, 2015

Revised: March 28, 2015

Published: March 30, 2015

In the present work, we used time-resolved absorption spectroscopy coupled with pulsed radiolysis in order, first, to study EDOT oxidation mechanism and, second, to definitely identify the nature of PEDOT growth process. This “fast” technique offers several advantages: it enables, via the pulsed electron accelerator, (i) the generation of oxidizing species in the aqueous irradiated medium in a very short time, (ii) the quantitative knowledge of oxidizing species concentration, (iii) the real-time following by absorption spectroscopy of the appearance and disappearance of transient species produced during EDOT oxidation and the estimation of the rate constants of the involved consecutive reactions. In particular we focused on the reaction of EDOT monomers with hydroxyl radicals produced by water radiolysis with the aim to identify the different transient and stable species involved in the first steps of HO<sup>•</sup>-induced PEDOT polymerization. Spectrokinetic analysis of experimental data and molecular simulations of absorption spectra were used as complementary methodologies to confirm the rate constants values and the transient and stable species identification.

With the aim to demonstrate the step-by-step PEDOT polymerization mechanism which we have already evoked and to synthesize conducting polymers by a new alternative method based on electron beam irradiation, we also used the electron accelerator as a “simple” electron irradiator: we irradiated EDOT solution using consecutive accumulated pulses to produce a high concentration in oxidative species for ensuring a quantitative polymerization of PEDOT. The resulting polymers were finally characterized by different physicochemical techniques in aqueous solution or after deposition onto substrates.

## ■ EXPERIMENTAL AND COMPUTATIONAL SECTION

**Chemicals.** Ethylenedioxothiophene (EDOT) monomer was purchased from Sigma-Aldrich. NaOH and HClO<sub>4</sub> used to adjust the pH value of the aqueous solutions were purchased from Analar NORMAPUR and Sigma-Aldrich, respectively. Distilled water (Millipore system 18.2 MΩ·cm) was used as solvent. Acetonitrile solvent ( $\geq$ 99.8%, Sigma-Aldrich) containing NOBF<sub>4</sub> (nitrosyl tetrafluoroborate, 97% purity, Sigma-Aldrich) as the dopant, was used during the electrical conductivity measurement.

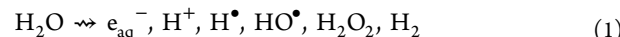
**Solution Preparation.** Aqueous solutions containing 1 mM or 10 mM in EDOT monomers were prepared. The natural pH of EDOT aqueous solutions is neutral, about 8. The pH was changed by adding HClO<sub>4</sub> to obtain acidic solutions at pH = 4, 5, and 6 or by adding NaOH to obtain alkaline solution at pH = 13. The pH was measured before and after irradiation, and only a slight decrease in the pH value was observed in the acidic and neutral solution, due to the production of H<sup>+</sup> ions during water radiolysis. All solutions were deaerated by bubbling with nitrous oxide, N<sub>2</sub>O, prior to irradiation, and then irradiated with an electron beam.

**Pulse Radiolysis Study.** The experiments were carried out on the picosecond laser-triggered electron accelerator ELYSE at University Paris-Sud (Orsay) coupled with a time-resolved absorption spectroscopic detection system.<sup>21,22</sup> The pulses were 4–6 nC, 15 ps, with an electron energy of 7.6 MeV, at a repetition frequency of 5 Hz. The dose per pulse was derived from the absorbance of the hydrated electron, e<sub>aq</sub><sup>−</sup>, at 660 nm at 3 ns with an extinction coefficient  $\epsilon_{660\text{ nm}} = 1.8 \times 10^4 \text{ L mol}^{-1} \text{ cm}^{-1}$  and a radiolytical yield of electron generation  $G(e_{\text{aq}}^-)_3\text{ ns} = 3.45 \times 10^{-7} \text{ mol J}^{-1}$ . For each pulse, the dose deposited in the aqueous irradiated volume was around 40 Gy (1 Gy = 1 J kg<sup>−1</sup>) (the

electron concentration being  $[e_{\text{aq}}^-] \approx 1.4 \times 10^{-5} \text{ mol L}^{-1}$ ). Due to the 2 to 5 mm diameter of the electron beam, the irradiated volume was around 100 μL. An N<sub>2</sub>O-purged stock solution of 200 mL was used which circulated in the 10 × 10 mm fused silica irradiation cell at a flow rate of 100 mL/min by means of a peristaltic pump. Since the electron pulses were applied at a frequency of 5 Hz, the solution was renewed between each pulse, and it was possible to apply up to 400 pulses for each kinetic measurement.

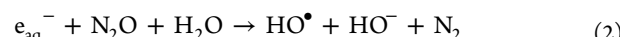
Absorption measurements were performed using the white light beam of a homemade xenon flash lamp.<sup>22</sup> The light was focused through the sample collinearly with the electron beam and then directed onto the slit of a flat field spectrograph (Chromex 250IS) equipped with three 150 grooves/mm grating blazed at 300, 500, and 800 nm which dispersed the light on the entrance optics of a streak-camera (model C-7700 from Hamamatsu). For this study, 100 ns, 1, 5, 50, 200 μs, and 1 ms sweep time/full screen were performed. For time range greater than 5 μs, a continuous 300 W Xe lamp was used. For each record of the streak-camera synchronized with the electron pulse, an image (1024 × 1344 pixels) resolved in time and wavelength (340 nm full screen) was acquired. However, to get a good signal-to-noise ratio, a series of 400 images were averaged in a unique image. Then, the time-resolved absorbance of the sample was calculated using average images obtained with and without the electron pulses. The full spectra from 245 to 850 nm were obtained by two series of absorption measurements using two different optical filters (UG5 and GG325) to optimize the light intensity on a specific spectral domain (250–400 and 360–700 nm, respectively). The spectral overlap between 360 and 400 nm allowed us to check the good stability and reproducibility of the irradiation measurements.

In pulsed radiolysis, a solution irradiated by a short pulse of high-energy electrons produces a significant concentration of radical species. If the system is an aqueous solution at neutral pH, under N<sub>2</sub> atmosphere, water radiolysis leads to the production of the following reactive species:



where the radiation chemical yields,  $G$  (mol J<sup>−1</sup>),<sup>23</sup> are as follows, respectively:  $G_{e_{\text{aq}}^-} = G_{\text{H}^+} = 2.65 \times 10^{-7} \text{ mol J}^{-1}$ ,  $G_{\text{H}^\bullet} = 0.60 \times 10^{-7} \text{ mol J}^{-1}$ ,  $G_{\text{HO}^\bullet} = 2.80 \times 10^{-7} \text{ mol J}^{-1}$ ,  $G_{\text{H}_2\text{O}_2} = 0.68 \times 10^{-7} \text{ mol J}^{-1}$ , and  $G_{\text{H}_2} = 0.45 \times 10^{-7} \text{ mol J}^{-1}$ .

Among the formed radical species, e<sub>aq</sub><sup>−</sup> and HO<sup>•</sup> are the most abundant species and have the higher reactivity, so the presence and reactivity of hydrogen atoms, H<sup>•</sup>, can be neglected. In the presence of N<sub>2</sub>O, e<sub>aq</sub><sup>−</sup> is efficiently converted into hydroxyl radical, HO<sup>•</sup>, through the following reaction:



Consequently, under N<sub>2</sub>O atmosphere, the radiolytic yield of HO<sup>•</sup> formation is doubled:  $G(\text{HO}^\bullet) = 5.45 \times 10^{-7} \text{ mol J}^{-1}$ . In these conditions, HO<sup>•</sup> is the only oxidizing species present in the system at a concentration of  $2.2 \times 10^{-5} \text{ mol L}^{-1}$  at about 100 ns for an absorbed dose of about 40 Gy. This radical is a powerful oxidant, having a standard redox potential of 2.7 V<sub>ESH</sub> in acidic solutions and 2.3 V<sub>ESH</sub> in neutral solutions.<sup>24,25</sup> Whatever the pH of the irradiated aqueous solutions, this radical is thus thermodynamically able to oxidize EDOT monomers, the redox potential of which amounts to 1.6–1.7 V<sub>ESH</sub>.<sup>14</sup>

**Electron Beam Irradiation.** In this study, the mechanism observed by pulsed radiolysis after one electron pulse suggested

that irradiation at higher dose should help to better understand the radiation-induced EDOT oxidation process. Practically, this was achieved by an electron beam irradiation of a static aqueous solution of EDOT, contained in a closed cell under the appropriate atmosphere, by a series of consecutive electron pulses at a frequency of 10 Hz. The absorption spectra of the solution were recorded, before, during, and after the electron beam irradiation.

**Characterization after Irradiation. UV–Visible Absorption Spectroscopy.** A HP 8543 spectrophotometer in the spectral range 200–1000 nm was used to record absorption spectra of EDOT solutions before and after pulsed radiolysis experiments or electron beam irradiations. In all cases, quartz cells with an optical length of 1 mm were used, and the reference was always pure water without any solute.

**Cryo-TEM microscopy.** Cryotransmission-electron microscopy (cryo-TEM), known to be adapted to low density contrast objects, was used to *in situ* characterize the structure of radiosynthesized PEDOT polymers in aqueous solution. A drop of irradiated solution was deposited on Quantifoil (Quantifoil Micro Tools GmbH, Germany) 200 mesh holey-carbon-coated grids. After being blotted with filter paper, the grids were rapidly quench-frozen by being plunged into liquid ethane. In this way, a thin ice film is formed, avoiding water crystallization and preserving polymer morphology in equilibrium in water. The grids were then transferred to the cryomicroscope, LaB6 JEOL JEM 2100 (JEOL, Japan), operating at 200 kV with a low dose system (minimum dose system, MDS) to protect the thin ice film from any irradiation before imaging and to reduce the irradiation during image capture. Images were recorded with an Ultrascan 2k CCD camera (Gatan, Pleasanton, CA).

**Lyophilization.** Irradiated samples were dried by lyophilization with a Heto PowerDry LL1500 (Thermo Electron Co., France) to obtain dehydrated powders. First, the solutions were transferred to culture dishes and frozen into ice. Then the frozen samples were moved to the drying chamber and lyophilized at  $-110\text{ }^{\circ}\text{C}$  for 48 h. Finally, the powders obtained after lyophilization were further investigated by attenuated total reflectance Fourier transform infrared spectroscopy (ATR-FTIR) and by scanning electron microscopy (SEM).

**ATR-FTIR Spectroscopy.** After irradiation, the identification of chemical composition of radiosynthesized PEDOT polymers was made by using ATR-FTIR spectroscopy using a Bruker Vertex 70 FTIR spectrometer with diamond ATR attachment (PIKE MIRACLE crustal plate diamond/ZnSe) and MCT detector with a liquid nitrogen cooling system. The dried powder, obtained by lyophilization, was deposited onto the ZnSe diamond, and then scanning was conducted from 4000 to  $400\text{ cm}^{-1}$  with a  $4\text{ cm}^{-1}$  spectral resolution. Each presented spectrum is an average of 100 scans.

**SEM Microscopy.** Scanning electron microscopy was used to check the morphology of radiosynthesized polymers after deposition. PEDOT powders obtained after lyophilization were sprinkled onto carbon tape adhered to aluminum mounts, and the images were recorded with an EVO MA10 scanning electron microscope supplied with SMRT SEM piloting program. Magnification, accelerating voltage, and scale bar were  $5000\times$ , 150 kV, and  $1\text{ }\mu\text{m}$ .

**Conductivity Test.** The PEDOT powder obtained by lyophilization was dissolved in an acetonitrile solution containing  $\text{NOBF}_4$  ( $10^{-2}\text{ mol L}^{-1}$ ) as chemical oxidant. Then a small drop of PEDOT-containing acetonitrile solution was deposited on a

glass slide and spined at 800 rpm for 60 s. This process was repeated three times, and a spin-coated film was obtained on the glass substrate. The thickness of the spin-coated film was then measured on a 3 Veeco Dektak 150 surface profiler. Finally, the electrical conductivity of the doped PEDOT film was conducted with a Kelvin four-point probe technique implemented with a Keithley 2420 system. All the measurements of thickness and conductivity were repeated three times, and an average value was calculated. The conductivity,  $\rho$  ( $\text{S cm}^{-1}$ ), was then determined using the following equation:

$$\rho = \left( \frac{\pi}{\ln(2)} \times \frac{V}{I} \times t \right)^{-1} \quad (3)$$

where  $V$  is the voltage difference (V),  $I$  is the applied current (A), and  $t$  is the thickness (cm).

**Computational Methods. Spectrokinetic Analysis.** Spectrokinetic analysis of the streak camera images was used to identify the number of distinguishable species and candidate reaction mechanisms. The methods and algorithms used has been presented in detail in a review paper by Ruckebusch et al.<sup>26</sup> The number of species is first estimated by singular value decomposition (SVD) of the image matrix, retaining only the components standing out of the noise. Then a parsimonious mechanism is proposed accordingly, and a hybrid soft-hard MCR-ALS algorithm is run to obtain the rate constants of the proposed mechanism and the spectra of the candidate species. In this procedure, the species kinetics are obtained by numerical or analytical integration of the differential equations of the reaction mechanism, while the spectra are obtained as numerical vectors subject only to positivity constraints. This results in smooth kinetics and noisy spectra.

Weighted least-squares are used to optimize the kinetic parameters and the spectra. The weight of each data point is the inverse of the *local* variance of the data, which is estimated on  $5 \times 5$  image cells as the variance of the residuals of a bilinear fit of the data. All points in a  $5 \times 5$  cell get the same weight. The quality of the fit is assessed on the SVD decomposition of the matrix of residuals. The mechanism is updated if necessary.

To perform a global analysis on the full range of times and wavelengths, streak camera images collected at different time scales (100 ns, 1  $\mu\text{s}$ , 5  $\mu\text{s}$ , 50  $\mu\text{s}$ , 200  $\mu\text{s}$ , and 1 ms) and wavelength scales (280–398 and 400–500 nm) were assembled into a single image. The intensity of individual images was slightly scaled to ensure the continuity of the kinetic traces within each wavelength scale. No wavelength-wise matching was performed.

All the calculations were made with codes developed in-house in the R environment.<sup>27</sup> Our hybrid MCR-ALS code is adapted from the ALS package,<sup>28</sup> with the *solvlp* constrained least-squares procedure from the *Rsolvp* package.<sup>29</sup>

**Molecular Simulations of the Radiolytic Species.** We performed molecular simulations based on Monte Carlo (MC) sampling of nuclear conformations and DFT calculations of the electronic energies. In our group, we have already used this approach for the simulation of radiolytic species.<sup>30</sup> In the present case the Monte Carlo sampling was performed in the following way:

1. For the EDOT monomers, adducts, and radicals, we performed an atomic sampling, with all the atoms moving independently.
2. For the neutral and cationic dimers, we supplemented the atomic sampling with a SCCS torsional sampling, enabling

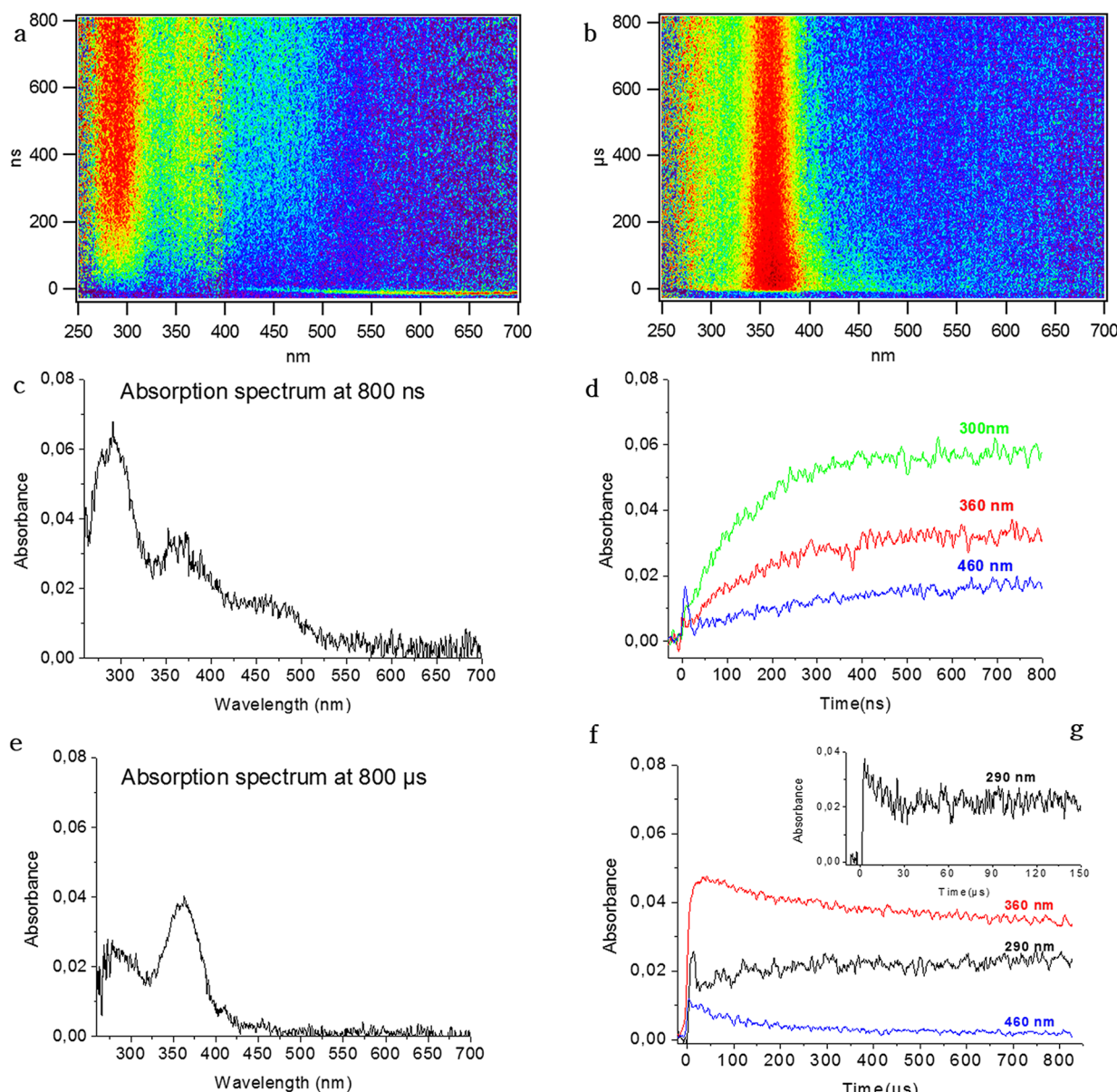


**Figure 1.** (a) Streak-camera image in the first 1  $\mu$ s after the pulse obtained by pulse radiolysis of an aqueous solution containing 1 mM in EDOT in a cell of 10 mm. (b) Streak-camera image in the first 1 ms after the pulse obtained by pulse radiolysis of an aqueous solution containing 1 mM in EDOT. (c) Optical absorption spectrum recorded 800 ns after the electron pulse. (d) Kinetic profiles over 1  $\mu$ s of the absorbancies at 300, 360, and 460 nm. (e) Optical absorption spectrum recorded 800  $\mu$ s after the electron pulse. (f) Kinetic profiles over 1 ms of the absorbancies at 290, 360, and 460 nm. (g) Kinetic profile over 150  $\mu$ s of the absorption at 290 nm.

the relative displacements of the monomers. This torsional move was given a probability 0.05.

All the DFT and TDDFT calculations were performed with the B3LYP functional<sup>31</sup> and the Dunning bases cc-pvdz (for the simulations) and aug-cc-pvdz (for the spectra).<sup>32</sup> Thermochemistry calculations were performed with the pSDD (polarized SDD) basis.<sup>33</sup>

Monte Carlo simulations were performed with the Gibbs program,<sup>34</sup> and electronic quantum calculations with the Gaussian 09 program.<sup>35</sup> The solvent was modeled with the SMD method.<sup>36</sup> No explicit solvent molecule was added to the bare solute.

The number of MC steps was currently set to 10 000. The spectra were calculated by a convolution of the first 20 TDDFT lines of a short list of configurations, according to the formula in

the literature.<sup>37</sup> This short list was built with one configuration out of 50 in the full MC list, after discarding the equilibration period. The convolution was made with gaussians with fwhm = 0.1 eV (full width at half-maximum).

## RESULTS AND DISCUSSION

**Kinetic Study of EDOT Oxidation.** A N<sub>2</sub>O-saturated aqueous solution containing 1 mM in EDOT at pH 8 was irradiated by an electron pulse with a dose of 40 Gy/pulse, and the time-resolved transient absorption spectra were measured at different time scales from 100 ns to 1 ms full scale. The streak camera images obtained in the first microsecond and in the first millisecond after the pulse are displayed in Figure 1a and Figure 1b, respectively. Figure 1c displays the absorption spectrum observed 800 ns after the electron pulse. The spectrum, which

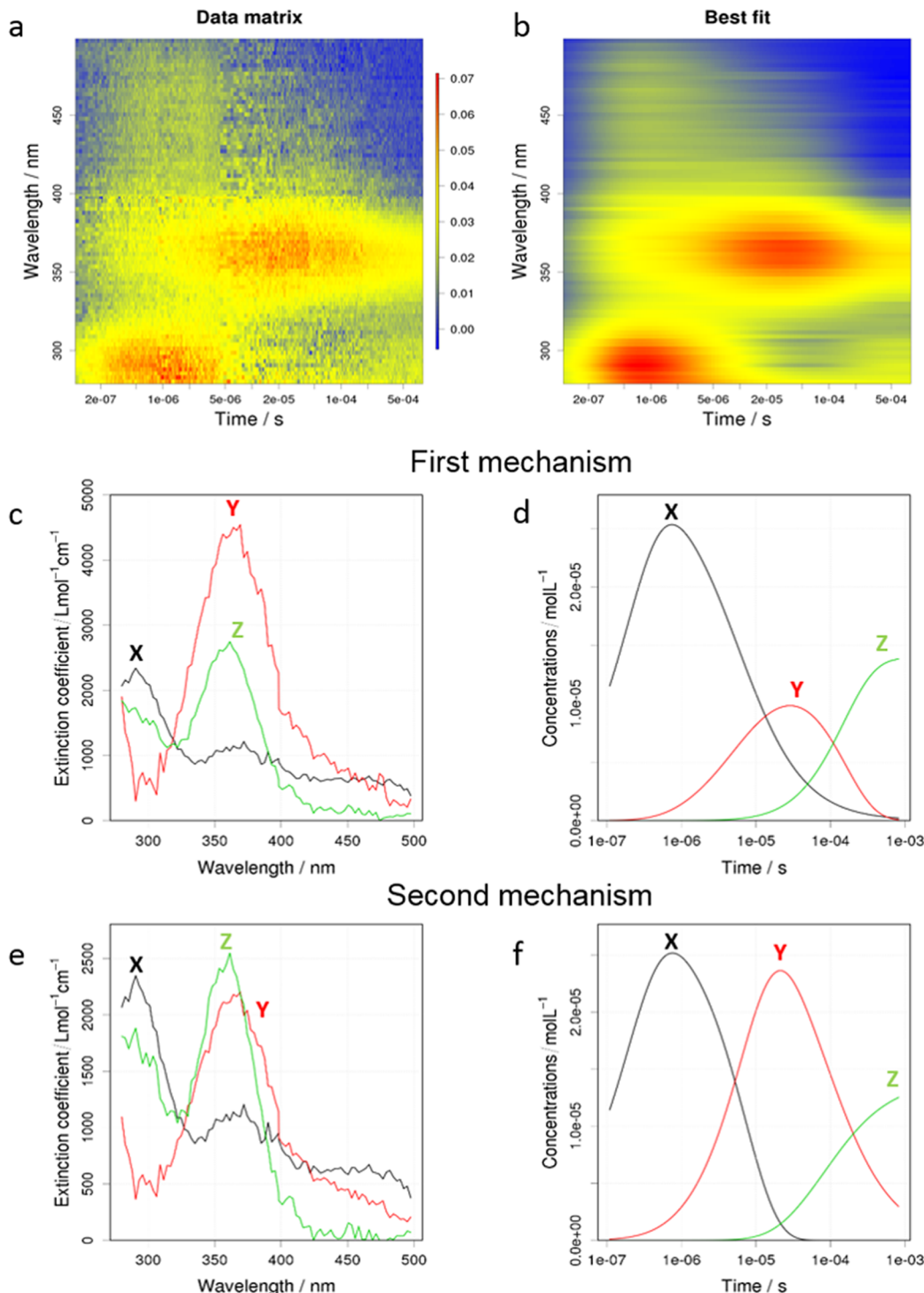


**Figure 2.** Kinetic analysis of the experimental spectrokinetic matrix (a) with a three-species model (see text); (b) image of the best-fit model; (c) best-fit spectra of the first model scheme; (d) best-fit concentrations for the first model scheme; (e) best-fit spectra of the second model scheme; (f) best-fit concentrations for the second model scheme. Each spectrum is associated with a concentration profile according to the color code.

should correspond to the first transient species produced through oxidation of EDOT by hydroxyl radical, exhibits three bands located at 300, 360, and 460 nm. The time evolution of these three absorption maxima is displayed in Figure 1d where the kinetic profiles are recorded on 1  $\mu$ s. The increase at 300 nm is the fastest, showing a quite rapid formation during 400 ns, and then it remains constant around its maximum until 800 ns. Differently, the two other bands at 360 and 460 nm demonstrate a continuous growth which is not over after 1  $\mu$ s. Note that the

kinetic profile at 460 nm is quite affected by the presence of a peak which corresponds to the fast decrease of hydrated electrons which absorb significantly at this wavelength and which are scavenged by N<sub>2</sub>O in around 10 ns (Figure 1d). In the literature, hydroxyl radical is well-known to form HO-adduct radicals onto C=C double bonds,<sup>38–41</sup> but it is also known to abstract either hydrogen atoms or electrons leading to neutral radicals or to cation radicals, respectively.<sup>42</sup> Starting from EDOT, we can then imagine the possible formation of three kinds of

radicals: EDOT-OH<sup>•</sup> adduct, EDOT<sup>•</sup> radical, and EDOT<sup>•+</sup> cation radical. Note that this latter species has often been proposed as the first radical involved in electrochemically induced EDOT polymerization<sup>6,43,44</sup>. However, at this stage of the study, it is difficult to distinguish how many species are involved in the absorption spectra, and therefore it is not possible to know their relative contribution to the kinetic profiles.

The evolution of these three bands was monitored for all time scales up to 1 ms. Note that at 1 ms, the longest time scale we can get, the absorption spectrum is characterized by only two peaks around 290 and 360 nm as shown in Figure 1e (800  $\mu$ s after the pulse). This species is a stable product formed after a one-pulse irradiation since we can observe it by static UV-vis absorption spectroscopy even some hours after the pulsed radiolysis experiments (figure not shown).

Over 1 ms, kinetic profiles were found to follow different trends. While at 5  $\mu$ s the kinetics of the peaks at 300 and 460 nm remain stable, the absorption at 360 nm is continuing to grow (profiles not shown here). This suggests that there are almost two transient species involved. When longer time scales (50 and 200  $\mu$ s) are investigated, the disappearance of the species at 460 nm is observed while the bands at 300 and 360 nm decay slowly. At the time scale of 1 ms, the kinetics of the three previous peaks observed at 460, 360, and 290 nm (Figure 1f) are completely changed. The peak at 460 nm disappears in 200  $\mu$ s, while that at 360 nm seems to have the same decay up to 200  $\mu$ s; but after this time it decreases more slowly (Figure 1g, inset of Figure 1f). This is probably due to the formation of some species absorbing at the same wavelengths. Finally, the peak at 300 nm decreases over 100  $\mu$ s, and then a new species is formed at 290 nm.

**Identification of Plausible Mechanism Schemes.** Spectrokinetic analysis of the streak camera images was performed in order first to identify the number of distinguishable species and second to propose candidate reaction mechanisms.

Figure 2a presents the composite image of several temporal scales corresponding to the aqueous solution of 1 mM in EDOT previously studied by pulsed radiolysis at pH 8. This image was used for global analysis. The SVD analysis of this image shows that the spectrokinetic matrix can be factored into three components. The best fit of the image obtained by the three-component model is shown in Figure 2b.

Two different mechanisms both involving, in addition to EDOT, three supplementary (X, Y, and Z) species can provide similar best-fit images. The spectra of the unknown X, Y, and Z species involved in both mechanisms (Figure 2c and Figure 2e) are strongly overlapping, and their kinetics are presented in Figure 2d and Figure 2f. The strong overlap found here, which we also already observed and evoked in the Kinetic Study of EDOT Oxidation section, makes necessary the use of a spectrokinetic analysis method to untangle the experimental data. Note that the shapes of the spectra of X, Y, and Z species recovered for both mechanisms differ mostly by the relative peak intensities; the peak positions remain identical for all species.

The first mechanism (Scheme 1) involves the following reactions:

### Scheme 1



The first reaction follows a pseudo-first-order kinetics since the amount of EDOT molecules is in excess in comparison with that of hydroxyl radicals. Note that in this mechanistic scheme, the second reaction follows a second-order kinetics, while the third one is a first- or a pseudo-first-order reaction.

In the second mechanism (Scheme 2), the successive reactions are as follows:

### Scheme 2



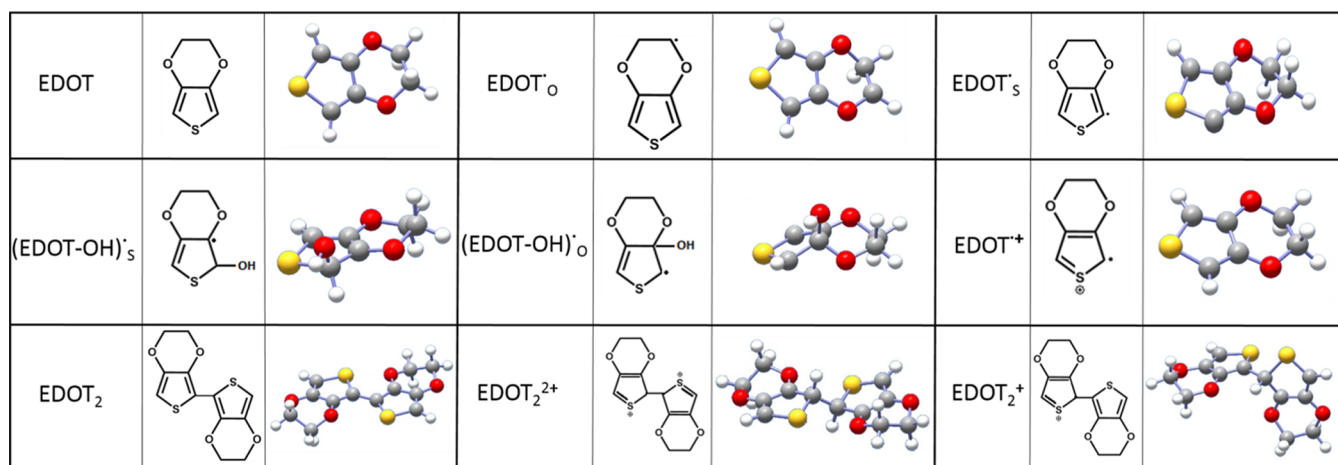
The first step is similar to that obtained in the previous Scheme. Nevertheless, contrarily to Scheme 1, the second reaction follows a first- or a pseudo-first-order kinetics, while the third one is a second order reaction.

From this analysis, we can conclude that in pulsed radiolysis of EDOT, two mechanistic schemes are plausible. In both schemes, the first and second species (X and Y, respectively) are transient species which disappear within 1 ms. The first species, X, which absorbs at 300, 360, and 460 nm is formed in the microsecond time scale. Then, in less than 100  $\mu$ s, X leads to the second species, Y, which absorbs at 360 nm. Finally, Y disappears at the millisecond time scale to form the third stable species, Z, which absorbs at 290 and 360 nm. This last species is the one we detected by pulsed radiolysis 1 ms after the pulse and which remains observable over a relatively long time after the end of the experiments.

**Computational Study of the Relevant Species.** The next step was to identify, through computational chemistry, the unknown X, Y, and Z species involved in the mechanism of EDOT oxidation and obtained by spectral deconvolution. Knowing that in both schemes (Schemes 1 and 2), the first reaction involves the reaction of EDOT with hydroxyl radical, the first transient species, X, should be one of the following species: EDOT-OH<sup>•</sup> adduct, EDOT<sup>•</sup> neutral radical, or EDOT<sup>•+</sup> cation radical. Then, taking into account that the disappearance of X leads to Y according to a monomolecular or bimolecular reaction and taking into account that Z is obtained from the first or second-order decay of Y, we considered all species which could be potentially produced according to Schemes 1 and 2. Some of these species which will be involved in the further discussion are represented in Table 1 (see also in Table 4 some of the reaction steps which should lead to these species).

In Table 1, we report the current names, formulas, and structures of all molecules of present interest. In Table 1 and further in the text, we follow the usual notation found in literature, which suffers from some ambiguities: in particular EDOT monomer and its cation radical EDOT<sup>•+</sup> differ by one electron, whereas EDOT<sub>2</sub> dimer and its radical cations EDOT<sub>2</sub><sup>+</sup> and EDOT<sub>2</sub><sup>2+</sup> differ by one and two protons, respectively. We checked that ionization of EDOT molecule removes an electron from the HOMO, which is a  $\pi$  orbital, mainly localized on both the carbon atoms in the  $\alpha$ -position of the S atom. Consequently, in EDOT<sup>•+</sup>, the S atom bears a positive charge (+0.74) as can be seen in Table 1. On another hand, we considered two EDOT<sup>•</sup> radicals, noted EDOT<sup>•</sup><sub>O</sub> and EDOT<sup>•</sup><sub>S</sub>, since two different H atoms, differently located in the EDOT molecule (in the  $\alpha$ -position of O atom or in the  $\alpha$ -position of S atom), can be abstracted by an hydroxyl radical. In the same way, we took into

Table 1. Name, Formula, and Chemical Structure of All Molecules of Interest

Table 2. Absorption Spectrum of EDOT Molecule: Measured and Calculated Values of the Absorption Maximum Wavelength (in nm), Extinction Coefficient (in L mol<sup>-1</sup> cm<sup>-1</sup>), and Band Width (in nm)

		exptl	MC	MC	MC	MD	MC
functional			B3LYP	B3LYP	B3LYP	B3LYP	BLYP
basis (simulation)			pSDD	cc-pvdz	cc-pvdz	cc-pvdz	cc-pvdz
basis (spectrum)			pSDD + diff	aug-cc-pvdz	aug-cc-pvdz	aug-cc-pvdz	aug-cc-pvdz
nbr of steps			10000	10000	50000	10 $\mu$ s	10000
spectrum	$\lambda_{\text{max}}$	255	243	250	250	253	282
	$E$	7048	19434	17454	17868	15604	11954
first band	$\lambda_{\text{max}}$	258	250	252	251	255	284
	$E$	5652	12535	14045	12505	12952	10601
	width	20	14	14	16	14	18
second band	$\lambda_{\text{max}}$	235	242	240	240	240	263
	$E$	5135	13586	9838	10149	10137	8347
	$\Delta\lambda_{\text{max}}$	23	8	12	11	15	21

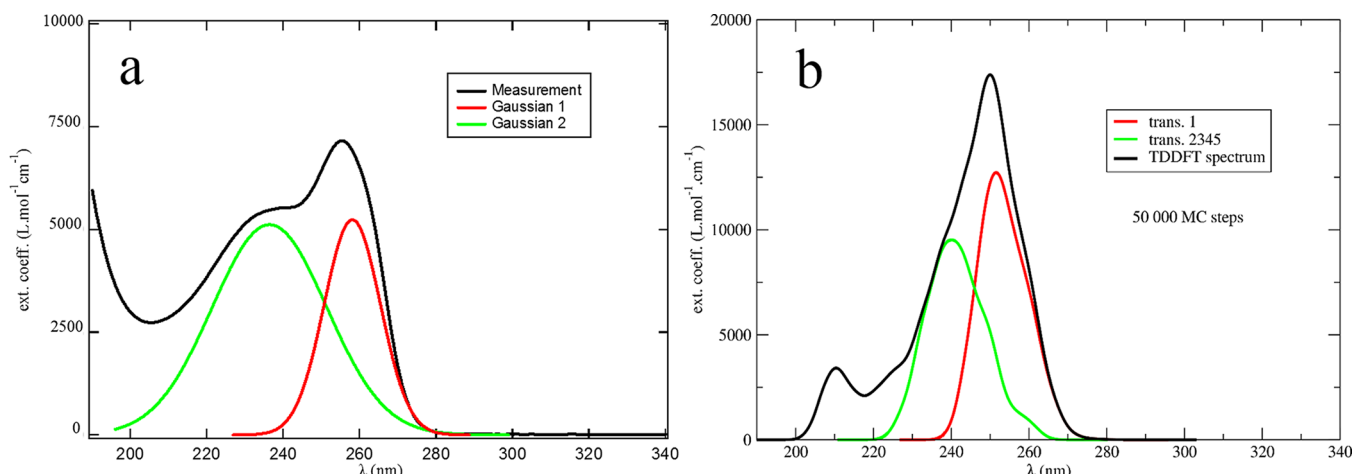


Figure 3. Absorption spectra of EDOT molecule: (a) experimental spectrum in aqueous solution (with a Gaussian fit) and (b) calculated spectrum with a MC simulation at the B3LYP/cc-pvdz level.

account the possible formation of two different adduct radicals: (EDOT-OH)<sup>•</sup><sub>s</sub> and (EDOT-OH)<sup>•</sup><sub>o</sub>.

To identify the unknown X, Y, and Z species, we decided to simulate the absorption spectra of the species displayed in Table 1 and then to compare them to the absorption spectra of X, Y, and Z found by spectrokinetic analysis. Before the extensive application of our simulation method, we established its relevancy in the following way: we first compared our simulation

possibilities for the EDOT molecule, for which the experimental spectrum is well-known. We then investigated the issue of the EDOT<sup>•+</sup> cation radical for which ordinary DFT calculations are doubtful.

**Absorption Spectrum of EDOT Molecule.** The absorption spectrum of EDOT is well-known.<sup>19</sup> It is characterized by two absorption maxima at 235 and 255 nm with the following extinction coefficients:  $\epsilon_{235} = 5650 \text{ L mol}^{-1} \text{ cm}^{-1}$  and  $\epsilon_{255} = 7048 \text{ L mol}^{-1} \text{ cm}^{-1}$ .

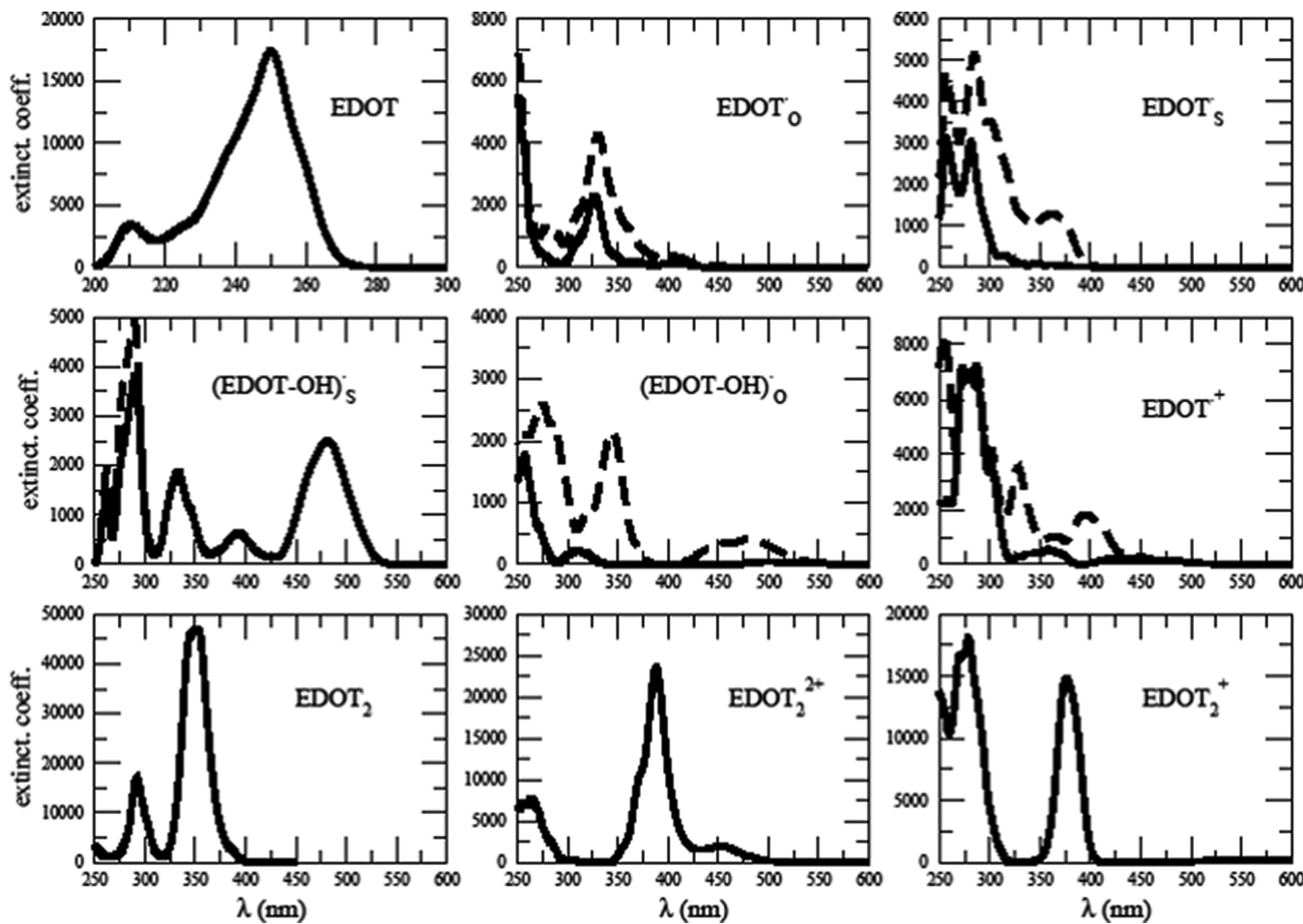


**Figure 4.** Absorption spectra of all molecules of Table 1. Absorption spectra of open shell radicals are displayed without (dotted line) and with (full line) spin screening with parameter 0.9.

$\text{L mol}^{-1} \text{cm}^{-1}$ . We compared several simulation methods on the case of EDOT molecule (Table 2). For an easier comparison, we made a fit of the recorded spectrum with three gaussians: the corresponding absorption wavelengths and molar extinction coefficients are given in Table 2.

We compared the Monte Carlo (MC) and Molecular Dynamic (MD)<sup>45</sup> simulations, different numbers of simulation steps, and the use of different functionals and basis sets. The results are given in Table 2, and the best Monte Carlo spectrum is shown in Figure 3b. For comparison with the experimental spectrum (Figure 3a), we extracted two bands from our calculated spectrum. We could easily attribute the first transition to a first band, but we had to gather the next four transitions (2 to 5) in the unique second band. We performed the B3LYP simulations with two basis sets:

1. The small pSDD basis set.<sup>46</sup> In this case the spectrum was calculated with the pSDD basis enriched with two shells of diffuse s and p gaussians on every atom.
2. The larger cc-pvdz basis. In this case the spectrum was calculated with the aug-cc-pvdz basis.

The results of Table 2 call for the following comments:

1. The results obtained with 10 000 and 50 000 MC steps show that the smaller number of MC steps (10 000) is sufficient. This results in reasonable simulation times for EDOT molecule and radicals (a few days each) and for the dimers (2–3 weeks each) on our eight core machines.

2. B3LYP yields acceptable values of the global  $\lambda_{\max}$  and the cc-pvdz basis yields the best values, 250 nm (with MC, error: 0.10 eV) and 253 nm (with MD, error: 0.04 eV)).
3. The MC and MD results are very close to each other, though MD results are slightly better. This suggests that our MC sampling is correct. Note that the use of molecular dynamics doubles computation times for the EDOT molecule.
4. B3LYP clearly overestimates the value of the extinction coefficient, by a factor 2.5 (with MC) and 2.2 (with MD).
5. We tested a few other functionals and found that only BLYP yields a smaller value of  $\epsilon$ : 12 000  $\text{L mol}^{-1} \text{cm}^{-1}$ . This value is still overestimated, and moreover the BLYP  $\lambda_{\max}$  is poor (282 nm).

An overestimated  $\epsilon$  may be due to at least the following issues:

1. The DFT transition dipole is inaccurate. We checked that the “velocity” and “position” values of the transition dipoles are very close to each other. According to the hypervirial theorem,<sup>47</sup> this shows that no numerical error interferes.
2. The DFT overestimates the transition dipole. Our group already published the case of an (inorganic) molecule for which B3LYP yields an oscillator strength larger than the (more correct) PBE value by a factor 2.<sup>46</sup> This discrepancy was due to an inaccurate B3LYP geometry. In the present case, we found that B3LYP overestimates the SC bond

lengths: the B3LYP optimized value (1.74 Å) is larger than the measured value (in the solid state, for a substituted molecule: 1.69–1.71 Å).<sup>48</sup> We found no noticeable influence of this bond length on the transition dipole, nevertheless.

3. The DFT potential surface is too rigid. A good measure of this rigidness is the value of the bandwidth: it can be seen that the value increases in the order B3LYP/pSDD < B3LYP/cc-pvdz < BLYP/cc-pvdz < measured value. We found that the value of the ZPE (zero point energy) of the molecule follows the same law: 0.111632 H (B3LYP/pSDD) < 0.111078 H (B3LYP/cc-pvdz) < 0.107345 H (BLYP/cc-pvdz). This shows that the potential surface is less and less rigid. We have no accurate value of this quantity, unfortunately.
4. The  $\epsilon$  value of the total spectrum depends on the overlap of the bands. It can be seen that the methods which give the best value of this quantity (MD/B3LYP and MC/BLYP) also give the largest separation of the two bands. It remains that the  $\epsilon$  value of the first band is overestimated in all cases.

Considering these issues, we adopted the following simulation method: we choosed the Monte Carlo method at the B3LYP/cc-pvdz level with 10000 MC steps, and the spectra at the B3LYP/aug-cc-pvdz level. We calculated in this way the spectra of all the closed shell species of Table 1, namely EDOT monomer and all dimers: EDOT<sub>2</sub>, EDOT<sub>2</sub><sup>+</sup> and EDOT<sub>2</sub><sup>2+</sup>. These spectra are gathered in Figure 4.

**Absorption Spectra of Open Shell Radicals.** Many of the radiolytic species of interest in the present work are doublet open shells, like EDOT<sup>•+</sup> radical cations, EDOT-OH<sup>•</sup> adducts, and EDOT<sup>•</sup> neutral radicals, with an H atom removed. We here face the issue that DFT and TDDFT methods usually use the UHF (unrestricted Hartree-Fock) formalism, which ensures that the projection  $M_S$  of the total spin can be monitored, but that its modulus  $S$  cannot. As a consequence the DFT wave functions of such systems display the right value  $|M_S| = 0.5$ , but the mean value of the  $S^2$  operator is not equal to  $S(S+1) = 0.75$ . Since it is due to the interference of quartet states, this feature has been called spin contamination.

In Table 3 we give the values of the  $\langle S^2 \rangle$  quantities for EDOT<sup>•+</sup> cation radical:

1. For the ground state, it amounts to 0.754, showing a weak spin contamination.
2. For excited states it is much larger, and values as large as 1.6 can be found, showing a strong contamination by quartet states. Note that for a pure quartet this value would be 3.75.

To analyze the TDDFT results, we used the SACCI method,<sup>49</sup> which handles true spin eigenfunctions and gives acceptable computation times. The SACCI results are joined to the TDDFT results in Table 3, as well as TDDFT results for the transitions between quartet states. To make the SACCI calculations feasible, we had to work in the vacuum and to drop diffuse gaussians from the basis sets, so that the results cannot be expected to be realistic. We only aimed at a comparison between two methods, free and not free from spin contamination.

The results of Table 3 call for the following comments:

1. The SACCI method only yields two weak transitions, before the intense one at 309 nm.

**Table 3. Comparison of the First Calculated Transitions of the Open Shell EDOT<sup>•+</sup> Cation Radical with SACCI (free from spin contamination) and TDDFT (not free)<sup>a</sup>**

method basis	doublets				quartets	
	$\Delta E$ (eV)	$\lambda$ (nm)	$f$	$\langle S^2 \rangle$	$\Delta E$ (eV)	$\lambda$ (nm)
SACCI cc-pvtz	0.84	1477	0.0005	0.75	-	-
	3.27	380	0.0002	0.75	-	-
	4.01	309	0.1502	0.75	-	-
	4.63	268	0.0032	0.75	-	-
	4.82	257	0.0343	0.75	-	-
DFT	0.	-	-	0.754	-	-
	0.55	2228	0.0004	0.767	-	-
	-	-	-	-	2.04	606
	-	-	-	-	2.38	519
	2.79	444	0.0008	0.791	2.84	436
	(3.19)	389	0.0177	1.598)	3.21	386
	-	-	-	-	3.29	376
	(3.68)	337	0.0034	1.045)	3.68	337
	-	-	-	-	3.72	333
TDDFT cc-pvdz	(3.85)	322	0.0224	1.468)	3.77	329
	4.12	300	0.0014	0.779	4.00	309
	4.68	264	0.1466	0.829	4.35	285

<sup>a</sup>These transitions are calculated at the optimized geometry in the vacuum. Bracketed transitions are discarded in the present work.

2. The TDDFT method yields a wealth of six weak transitions before the intense one (at 264 nm), with  $\langle S^2 \rangle$  values lying between 0.77 and 1.6.
3. A great number of quartet states exist in the zone of spin contamination and may interfere.

The TDDFT spectra for  $|M_S| = 0.5$  and 1.5 are shown in Figure 5. The TDDFT results can be made closer to the SACCI results if the transitions with a  $\langle S^2 \rangle$  value larger than some value, say 0.82, are dropped from the list. These discarded lines are bracketed in Table 3. Doing so, we obtain the “screened” spectrum of Figure 5. In this figure we join the “spectrum” of the  $\langle S^2 \rangle$  values, namely the equivalent of the absorption spectrum, with the oscillator strength replaced by the  $\langle S^2 \rangle$  value. This  $\langle S^2 \rangle$  spectrum was normalized, so as to give the value 0.75 to the low energy band (2228 nm, see Table 3):

1. The band at 400 nm in the crude spectrum can be attributed to quartet states, as shown by the large value of  $\langle S^2 \rangle$  in this zone (1.72) and by a band in the quartet spectrum. As a consequence, this band is completely dropped by the spin screening.
2. The same holds for the band at 330 nm, also displaying a large value of  $\langle S^2 \rangle$  (1.88) and clearly present in the quartet spectrum.

In Figure 4, we gathered the spectra of five open shell species of present interest:

1. For EDOT<sup>•+</sup> cation radical, the spin screening dramatically modifies the crude TDDFT spectrum, as already discussed.
2. This is also the case for the two neutral radicals EDOT<sup>•</sup> and EDOT<sup>•</sup><sub>S</sub>, and for the (EDOT-OH)<sup>•</sup><sub>O</sub> adduct.
3. On the other hand, the spin screening leaves the spectrum of the (EDOT-OH)<sup>•</sup><sub>S</sub> adduct almost invariant, at least in the low energy zone.

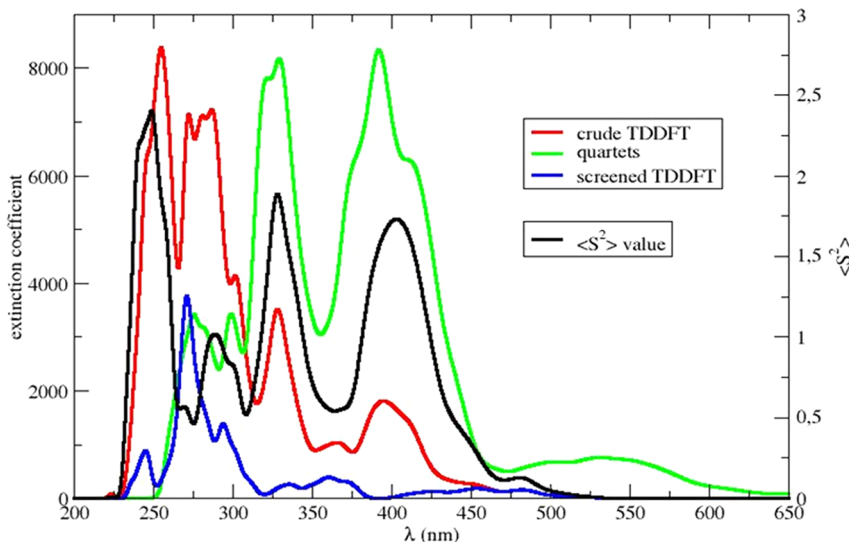


**Figure 5.** Absorption spectra of EDOT $\bullet^+$  radical cation: TDDFT results for  $M_S = 0.5$  (“crude” spectrum) and 1.5 (“quartet” spectrum) and screened TDDFT spectrum with the value 0.82 of the screening parameter. The “spectrum” of the  $\langle S^2 \rangle$  mean value for the crude TDDFT spectrum is also shown.

The results of the spin screening procedure obviously depend on the value of the threshold. In Figure 5 we display the spectrum of EDOT $\bullet^+$  cation radical obtained with the value 0.82 which ensures the best comparison with the experimental spectrum. In Figure 4 we use the value 0.9 because the extinction coefficients are larger and the absorption spectra more visible.

**Thermochemistry of the Candidate Reactions.** Simulated absorption spectra suffer from the DFT inaccuracies, and moreover these spectra often overlap, so that thermochemical data are most welcome in the further discussion with the aim to identify X, Y, and Z species and also the effective mechanism scheme.

In Table 4 we give the *molar* free energy change  $\Delta_r G^m$  of a list of chemical reactions, relevant to the present study. All the calculations were performed with B3LYP and the pSDD basis set. In a previous work, our group had shown that PCM (polarized continuum) methods, such as SMD, can be very unreliable and hazardous when used for chemical reactions of the type  $A + B \rightarrow C$  or  $A \rightarrow B + C$ .<sup>50</sup> This is due to the poor treatment of the translation rotation entropy, which is given an electrostatic additivity in PCM methods. Consequently, we used the following methods:

For all  $A + B \rightarrow C + D$  reactions, we used the SMD method; the free energy change for such a reaction is therefore

$$\Delta_r G^m = E_{\text{smd}}(C) + E_{\text{smd}}(D) - E_{\text{smd}}(A) - E_{\text{smd}}(B) \quad (9)$$

where  $E_{\text{smd}}$  is the energy in the dielectric cavity. Using full free energies  $G_{\text{smd}}$  in eq 9 yields only tiny differences.

For  $A + B \rightarrow C$  reactions, where all species are neutral, we calculated the free energy changes in the vacuum:

$$\Delta_r G^m = G_{\text{vac}}(C) - G_{\text{vac}}(A) - G_{\text{vac}}(B) \quad (10)$$

where the  $G_{\text{vac}}$  are the full free energies in the vacuum, including in particular the vibration, rotation, and translation entropies. We think that using vacuum quantities is less hazardous than using PCM quantities in this case.

For  $A + B \rightarrow C$  reactions, where some species bear an electrostatic charge, we calculated the free energy changes in the vacuum and added a solvation contribution given by the Born formula and the sphere radius deduced from the electron density.<sup>51</sup>

$$\begin{aligned} \Delta_r G^m = & G_{\text{vac}}(C) - G_{\text{vac}}(A) - G_{\text{vac}}(B) + \Delta G_{\text{solv}}(C) \\ & - \Delta G_{\text{solv}}(A) - \Delta G_{\text{solv}}(B) \end{aligned} \quad (11)$$

In Table 4 we give the molar values of the free energy change and the corresponding values at pH = 7, with all species (other than H $^+$ ) molar. The first three reactions R1 to R3 of Table 4 are simple association reactions between EDOT and hydroxyl radical. The reactions R4 to R8 correspond to all candidate reactions of HO $\bullet$  radical with EDOT molecule. Thus, one of these reactions (R4 to R8) necessarily corresponds to reaction 4 involved in both Schemes 1 and 2, reaction which yields the first transient species X. The reactions R9 to R17 of Table 4 are the monomolecular and bimolecular reactions which could happen if the first transient species X was identified as EDOT $\bullet^+$  radical cation. Since X is indeed shown to be EDOT $\bullet^+$  (as demonstrated in next section), all the reactions which describe the disappearance of all the other candidates for X species, namely EDOT $\bullet_O$ , EDOT $\bullet_S$ , (EDOT-OH) $\bullet_S$ , and (EDOT-OH) $\bullet_O$  have been omitted from Table 4 for clarity. Then, among the reactions R9 to R17, one can find the reactions 5 and 6 or 7 and 8 which follow reaction 4 in Schemes 1 and 2, respectively.

#### Mechanism Determination and Species Identification.

The last step of the present investigation was to definitely identify the species and consequently to describe the EDOT oxidation mechanism. Figure 3 shows that the spectrum of EDOT $^{19}$  is well reproduced by the simulation. Otherwise, the absorption spectrum of the first species X produced by the reaction between EDOT monomer and hydroxyl radical, as deduced by spectrokinetic analysis (Figure 2), displays three peaks at 300, 360, and 460 nm. As it was already explained, X is one of the following species: (EDOT-OH) $\bullet_S$ , (EDOT-OH) $\bullet_O$ , EDOT $\bullet^+$ , EDOT $\bullet_S$  or EDOT $\bullet_O$  which could be respectively formed by the reactions R4, R5, R6, R7, or R8 of Table 4. According to the molar free energies values corresponding to these reactions (Table 4), except reaction R7 which is not favored due to a positive  $\Delta_r G^m$ , all the reactions are thermodynamically possible at neutral pH. Then, except EDOT $\bullet_S$ , all the other radical species could be formed. By comparing the simulated spectra of all these species displayed in Figure 4 with that of X found by spectrokinetic analysis (Figure 2) and with the crude

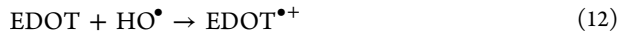
Table 4. Thermochemistry of Some Chemical Reactions Relevant to the Present Work<sup>a</sup>

	reaction step	comment	$\Delta_r G^m$	$\Delta_r G^m$ (pH = 7)	environment
R1	EDOT + HO <sup>•</sup> → EDOT...HO <sup>•</sup>	transition state	+0.179		vacuum
R2	EDOT + HO <sup>•</sup> → EDOT...HO <sup>•</sup>	S...O VdW complex	+0.115		vacuum
R3	EDOT + HO <sup>•</sup> → EDOT...HO <sup>•</sup>	O...H H-bond	+0.136		vacuum
R4	EDOT + HO <sup>•</sup> → (EDOT-OH) <sup>•</sup> <sub>s</sub>	adduct	-0.874		vacuum
R5	EDOT + HO <sup>•</sup> → (EDOT-OH) <sup>•</sup> <sub>o</sub>	adduct	-0.370		vacuum
R6	EDOT + HO <sup>•</sup> → EDOT <sup>•+</sup> + HO <sup>-</sup>	charge transfer	+0.301	-0.13	water
R7	EDOT + HO <sup>•</sup> → EDOT <sup>•</sup> <sub>s</sub> + H <sub>2</sub> O	H abstraction	+0.042		water
R8	EDOT + HO <sup>•</sup> → EDOT <sup>•</sup> <sub>o</sub> + H <sub>2</sub> O	H abstraction	-0.917		water
R9	EDOT <sup>•+</sup> → EDOT <sup>•</sup> <sub>s</sub> + H <sup>+</sup>	deprotonation	+1.266	+0.86	water
R10	EDOT <sup>•+</sup> → EDOT <sup>•</sup> <sub>o</sub> + H <sup>+</sup>	deprotonation	+0.306	-0.10	water
R11	EDOT <sup>•+</sup> + EDOT → EDOT <sub>2</sub> <sup>•+</sup> + H <sub>2</sub>	dimerization	-0.331		water
R12	EDOT <sub>2</sub> <sup>•+</sup> + EDOT → EDOT <sub>2</sub> <sup>+</sup> + EDOT <sup>•+</sup>	charge transfer	+0.803		water
R13	EDOT <sup>•+</sup> + EDOT → EDOT <sub>2</sub> <sup>+</sup> , H	dimerization	+0.404		water
R14	EDOT <sup>•+</sup> + EDOT <sup>•+</sup> → EDOT <sub>2</sub> <sup>2+</sup>	dimerization	-0.743		water
R15	EDOT <sub>2</sub> <sup>2+</sup> → EDOT <sub>2</sub> <sup>+</sup> + H <sup>+</sup>	deprotonation	-0.676	-1.09	water
R16	EDOT <sub>2</sub> <sup>+</sup> → EDOT <sub>2</sub> <sup>+</sup> + H <sup>+</sup>	deprotonation	-0.521	-0.93	water
R17	EDOT <sup>•+</sup> + EDOT <sup>•</sup> <sub>s</sub> → EDOT <sub>2</sub> <sup>+</sup>	dimerization	-1.712		water
R18	EDOT + O <sup>•-</sup> → EDOT <sup>•</sup> <sub>s</sub> + OH <sup>-</sup>	H abstraction	+0.375		water
R19	EDOT + O <sup>•-</sup> → EDOT <sup>•</sup> <sub>o</sub> + OH <sup>-</sup>	H abstraction	-0.584		water
R20	EDOT + O <sup>•-</sup> → EDOT-O <sup>•-</sup> (open cycle)	adduct	-1.852		vacuum

<sup>a</sup>The  $\Delta_r G^m$  are molar reaction free energies (in eV), calculated with the B3LYP functional and the pSDD basis set.

experimental spectrum at 800 ns (Figure 1b), one can conclude that only EDOT<sup>•+</sup> and (EDOT-OH)<sup>•</sup><sub>s</sub> are plausible candidates. In fact, the neutral radical EDOT<sup>•</sup><sub>o</sub> has only one peak at 325 nm while the (EDOT-OH)<sup>•</sup><sub>o</sub> radical absorbs significantly at about 300 nm.

For the first species X, we have only two plausible candidates: the EDOT<sup>•+</sup> cation radical and the (EDOT-OH)<sup>•</sup><sub>s</sub> radical adduct since their spectra present three absorption maxima around 300, 360, and 460 nm (Figure 4) such as X species (Figure 2). Nevertheless, one can observe that the spectrum of X fits better with that of EDOT<sup>•+</sup>. In particular the third absorption band located at around 460 nm is less intense than the other absorption bands. On the contrary, the peak at 460 nm is more intense than the other ones in the case of (EDOT-OH)<sup>•</sup><sub>s</sub>. This suggests that the first X species is EDOT<sup>•+</sup> radical cation, formed according to reaction R6 of Table 4 which has a negative value of  $\Delta_r G^m$  (-0.13 eV at pH = 7). This is in good agreement with literature reports where the presence of EDOT<sup>•+</sup> is often suggested.<sup>6,13,43,44</sup> The absence of (EDOT-OH)<sup>•</sup><sub>s</sub> adduct may still be explained. Indeed, it can be seen from reactions R1 to R3 of Table 4 that the approach of a hydroxyl radical involves the crossing of a potential barrier larger than 0.1 eV. Then, even if the adduct formation (R4 of Table 4) is possible due to its negative free energy, it is certainly made very slow by this large potential barrier. On the other hand, charge transfer reactions may occur at large distances, so that potential barriers have no effect, which should explain the preferential (faster) formation of EDOT<sup>•+</sup> according to



Evidently, this reaction corresponds to reaction 4 previously evoked in Schemes 1 and 2.

Starting from EDOT<sup>•+</sup>, reactions R9 to R17 of Table 4 are the monomolecular and bimolecular reactions which could further happen and lead to the unknown Y species which absorbs at 360 nm. Among all these reactions, according to Scheme 2, we can retain unimolecular reactions (R9 and R10) as well as pseudo-first-order reactions (R11 and R13) as candidate steps for

reaction 7, while according to Scheme 1, we can retain bimolecular reaction (R14) as a candidate step for reaction 5. Note that the other second-order reactions of Table 4 must be excluded since, according to Scheme 1, X should react on itself in reaction 5 leading to the last unknown Z species.

Unimolecular reactions (R9 and R10) which should lead to the neutral radicals (EDOT<sup>•</sup><sub>s</sub> or EDOT<sup>•</sup><sub>o</sub>) must be excluded from the candidate mechanism. Indeed, EDOT<sup>•</sup><sub>s</sub> cannot be formed since the molar free energy value corresponding to reaction R9 is positive (Table 4), while EDOT<sup>•</sup><sub>o</sub> spectrum displays an absorption maximum at 325 nm which is far from the maximal absorption of Y species. Besides, concerning pseudo-first-order reactions which could be involved in Scheme 2, reaction R13 must be excluded since the corresponding molar free energy value is positive (Table 4). Contrarily to reaction R13, reaction R11 which also implies the action of EDOT<sup>•+</sup> onto EDOT monomer is thermodynamically favored since the corresponding  $\Delta_r G^m$  is negative. Nevertheless, a high barrier and a very low reaction rate must be expected because such a reaction needs the breaking of two C-H bonds before the formation of H<sub>2</sub> product. For this reason, we consider that reaction R11 is very unlikely to occur in our time window. Thus, Scheme 2 must be excluded and X necessarily disappears according to the second-order reaction R14 of Table 4:



Evidently, this reaction which is thermodynamically favored (very negative  $\Delta_r G^m$  value, see Table 4) corresponds to reaction 5 of Scheme 1. This dimerization results from the bond formation between two C atoms, each bearing an unpaired electron, as can be seen in Table 1. Thus, the species Y must be identified as the EDOT<sub>2</sub><sup>2+</sup> dimer cation. This is definitely confirmed by the fact that Y spectrum (Figure 2c) is very similar to EDOT<sub>2</sub><sup>2+</sup> simulated one (Figure 4).

Finally, we focus on the last step of Scheme 1. This reaction 6 is monomolecular and leads, starting from EDOT<sub>2</sub><sup>2+</sup>, to the Z stable species which absorbs at 290 and 360 nm (Figure 2). Note that this absorption is far from the well-known optical absorption

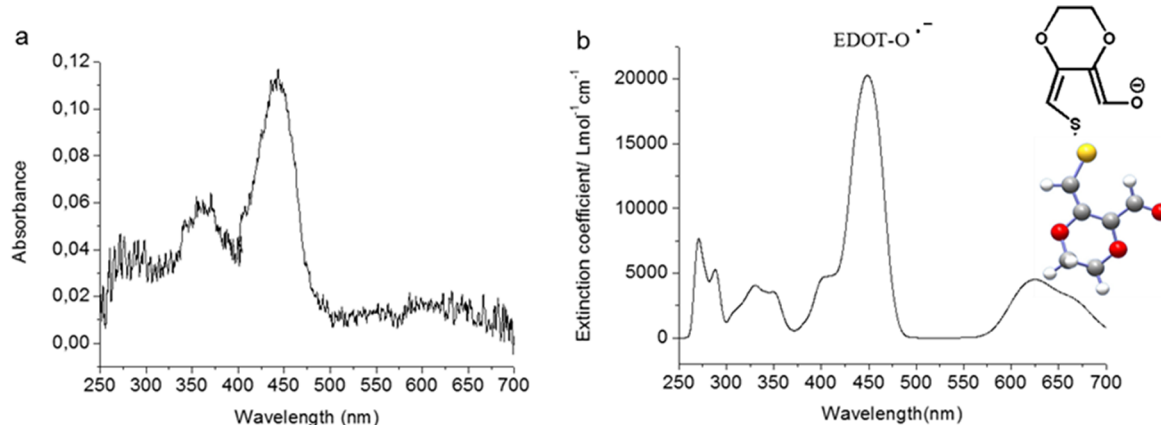
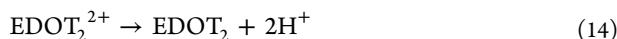


**Figure 6.** (a) Experimental absorption spectrum of a solution containing 1 mM in EDOT at pH 13 recorded 25  $\mu$ s after the pulse. (b) Simulated spectrum of the open cycle species formed by the reaction between EDOT and the oxide radical.

of PEDOT polymers<sup>53</sup> which has been reported around 600 nm. In literature, a pulsed radiolysis study concerning thiophene molecules<sup>38,39</sup> ( $\text{Th}$ , a molecule very similar to EDOT) demonstrated that thiophene dimers ( $\text{Th}_2$ ) are characterized by two absorption bands at 301 and 406 nm. In a previous study,<sup>20</sup> in which PEDOT was synthesized by using  $\gamma$ -irradiation, our group showed that  $\text{EDOT}_2$  dimer is a stable product and displays also two absorption bands at 290 and 360 nm (slightly displaced in comparison with those of  $\text{Th}_2$ ). In agreement with these results and since the absorption maxima of  $\text{EDOT}_2$  correspond to those of Z, we supposed in the present work that  $\text{EDOT}_2$  dimer is the last unknown stable Z species produced by pulsed radiolysis. This is definitely confirmed by the fact that the Z spectrum (Figure 2c) is very similar to both the simulated  $\text{EDOT}_2$  spectrum (Figure 4) and the experimental spectrum obtained by pulsed radiolysis 800  $\mu$ s after the pulse (Figure 1e). Thus, the last step involved in the experimental mechanism corresponds to the deprotonation of  $\text{EDOT}_2^{2+}$  according to



Note that this reaction which corresponds to reaction 6 of Scheme 1 is thermodynamically favored at pH = 7. Indeed, it corresponds to the sum of two thermodynamically favored reactions (R15 and R16 of Table 4).

In conclusion, the mechanism of EDOT oxidation initiated by hydroxyl radical leads to  $\text{EDOT}_2$  dimer according to the mechanistic Scheme 1 made up of the consecutive reactions 12, 13, and 14. The mechanism proposed here may neglect the formation of other minority species which could be also produced during EDOT oxidation. In particular, we could suppose the formation of small amounts of  $(\text{EDOT}-\text{OH})^\bullet_s$  adduct radical, which is thermodynamically favored, and thus the potential contribution of this additional species to the spectrum which we globally attributed to  $\text{EDOT}^\bullet+$ . Unfortunately, it is not possible for us to distinguish such minority species.

Spectrokinetic analysis enabled the fit of the variation of X, Y, and Z concentrations over time. Thus, it enabled the evaluation of the rate constants  $k_{12}$ ,  $k_{13}$ , and  $k_{14}$  of reactions 12, 13, and 14 respectively. The best-fit values are

$$k_{12} = 4.8 \times 10^9 \text{ L mol}^{-1} \text{ s}^{-1} \quad (15)$$

$$k_{13} = 3.4 \times 10^9 \text{ L mol}^{-1} \text{ s}^{-1} \quad (16)$$

$$k_{14} = 7000 \text{ s}^{-1} \quad (17)$$

Due to the possible presence of minority species, not taken into account in the spectrokinetic analysis, these rate constant values could be overestimated.

**Effect of pH on EDOT Oxidation.** Up to now, we have considered oxidation of EDOT by hydroxyl radical at pH = 8. Indeed, the pulsed radiolysis experiments as well as the spectrokinetic analysis were conducted at this neutral pH. The evidenced scheme mechanism made up of the consecutive reactions 12, 13, and 14 is thus that which occurs in neutral aqueous medium. Nevertheless, one can see in Table 4 that many reactions which could occur during EDOT oxidation involve hydronium or hydroxide ions. Such reactions are pH-sensitive and should be thermodynamically displaced when the pH is changed. Moreover, an increase in pH value should favor the stabilization and then the observation of  $\text{EDOT}-\text{OH}^\bullet$  adducts the dehydration of which is favored at low pHs leading to  $\text{EDOT}^\bullet+$  cation radicals.

To check whether the pH variation affects the oxidation mechanism of EDOT, we changed the initial pH of the aqueous solution containing EDOT monomers.  $\text{N}_2\text{O}$ -saturated aqueous solutions containing 1 mM in EDOT at different pHs (4, 5, 6, and 13) were then irradiated by an electron pulse with a dose of 40 Gy/pulse, and the time-resolved transient absorption spectra were recorded by pulsed radiolysis at each pH.

The results we got at acidic pHs (4, 5, and 6) were similar and identical to those obtained at pH = 8. The spectral evolution and the kinetics found were exactly those already described in the paper. Thus, at pHs lower than 8, no pH effect was found and no  $\text{EDOT}-\text{OH}^\bullet$  adduct was detected. Whatever the pH value in neutral or acidic conditions, the mechanistic scheme is always made up of reactions 12, 13, and 14 and indifferently leads to  $\text{EDOT}_2$  dimer.

On the contrary, the kinetic and spectral results we got in alkaline media (results not shown) were rather different from those obtained in acidic or neutral conditions. This is due to the fact that when the pH of the solution increases,  $\text{HO}^\bullet$  is progressively transformed into its conjugated alkaline form, namely oxide radical  $\text{O}^\bullet-$ . When the pH becomes higher than 11.8 ( $\text{pK}_a(\text{HO}^\bullet/\text{O}^\bullet-)$  value),<sup>54</sup>  $\text{O}^\bullet-$  radicals become predominant in the medium, and at pH = 13, their concentration reaches 16 times that of  $\text{HO}^\bullet$  hydroxyl radicals.

The time-resolved spectral evolution of the EDOT solution irradiated at pH = 13 was different from those obtained at pHs lower than 8. Neither the characteristic peaks of  $\text{EDOT}^\bullet+$  cation radical nor those of  $(\text{EDOT}-\text{OH})^\bullet_s$  adduct were observed.

Differently, a transient species whose absorption maxima were located at 350, 430, and 625 nm was predominantly observed at all time scales (Figure 6a). Evidently, this species is that produced through the reaction of EDOT with O<sup>•-</sup> oxide radical. Some of the possible reactions between these two reactants (R18, R19, and R20) are specified in Table 4.

Thermochemical calculations (see Table 4) demonstrated that among all the candidate reactions between EDOT and O<sup>•-</sup>, the addition reaction R20 is the more favorable since its molar free energy is very negative:  $-1.85\text{ eV}$ . Note that the geometry optimization of the adduct formed by this reaction, namely EDOT-O<sup>•-</sup>, yielded a ring opening. The open cycle produced is represented in the inset of Figure 6b. So that it is very likely that the O<sup>•-</sup>-adduct does not exist. These results were confirmed by simulation of the absorption spectrum of the open cycle since the experimental spectrum recorded 25  $\mu\text{s}$  after the pulse (Figure 6a) is in a very good agreement with the simulated one (Figure 6b). The present results which concern the EDOT ring opening are also in good agreement with a previous study which concerned thiophene (Th) oxidation.<sup>38,39</sup> In fact, the authors found that the action of oxide radicals onto Th in alkaline solution induces a ring opening which leads to a species which absorbs at around 430 nm.

We can conclude that the action of the oxide radical produced by water radiolysis in alkaline solutions onto EDOT monomers leads to an open cycle preventing any dimerization of EDOT and consequently any polymerization of PEDOT. Note that, even if some residual HO<sup>•</sup> radicals remain in the alkaline medium at pH = 13, their potential action onto EDOT was not distinguishable. Neither EDOT<sup>•+</sup> cation radical nor EDOT-OH<sup>•</sup> adduct were observed in these alkaline conditions. Note also that if EDOT-OH<sup>•</sup> was formed in alkaline medium, it should quickly deprotonate leading to EDOT-O<sup>•-</sup> adduct and thus to the open cycle.

#### EDOT<sub>2</sub> Dimer as a Stable Product of Pulsed Radiolysis.

**A Discussion.** Contrarily to alkaline solution where no dimerization of EDOT can happen, in acidic and neutral aqueous media, the pulsed radiolysis-induced oxidation of EDOT by hydroxyl radical leads first to a transient species, namely EDOT<sup>•+</sup>, which dimerizes and deprotonates, leading to an unique stable product: EDOT<sub>2</sub> dimer that we can observe and characterize over a long time after the experiments. Nevertheless, no polymerization took place after one pulse (40 Gy) irradiation. No other products such as EDOT oligomers were obtained. These experimental facts can be explained by the following considerations:

1. PEDOT polymerization is not a chain reaction. If it was the case, EDOT<sup>•+</sup> cation radicals would react first with EDOT monomers leading to EDOT<sub>2</sub><sup>•+</sup> and then to EDOT<sub>2</sub> according to reactions R11 and R12 of Table 4. However, such reactions are not observed. EDOT<sup>•+</sup> cation radicals would then react with all the following EDOT<sub>n</sub> oligomers, generating successive EDOT<sub>n+1</sub><sup>•+</sup> cation radicals and EDOT<sub>n+1</sub> oligomers. This would imply, after one pulse irradiation, the presence of many species. But it is clearly not the case.

2. PEDOT polymerization proceeds through a step-by-step process made up of recurrent oxidation (activation)/growth (chain length increase)/deprotonation steps. If it is the case, EDOT monomers are first oxidized by hydroxyl radicals into EDOT<sup>•+</sup> radical cations which dimerize and deprotonate, leading to EDOT<sub>2</sub> dimers. This first step is effectively observed. Then, at each step of the process, EDOT<sub>n</sub> and EDOT<sub>m</sub> oligomers are oxidized by hydroxyl radicals into EDOT<sub>n</sub><sup>•+</sup> and EDOT<sub>m</sub><sup>•+</sup>

radical cations which react together, ensuring the chain length increase and thus the polymerization, by forming EDOT<sub>n+m</sub><sup>2+</sup> transient species which then deprotonate, leading to longer EDOT<sub>n+m</sub> oligomers. Such a recurrent mechanism is thermodynamically acceptable since the oxidizability of EDOT oligomers increases with their chain length. However, no oligomers longer than EDOT<sub>2</sub> dimers were observed in our experimental conditions after one pulse of 40 Gy. Nevertheless, this can be explained as follows: during pulsed radiolysis experiments, the concentration of hydroxyl radicals produced during one pulse of 40 Gy ( $2.2 \times 10^{-5}\text{ mol L}^{-1}$ ) is nearly 50 times smaller than that of EDOT monomers (1 mM). Yet, the quantitative oxidation of EDOT into EDOT<sub>2</sub> needs at least 1 mM in HO<sup>•</sup>. The amount of hydroxyl radicals generated in one pulse is definitely not sufficient to totally transform EDOT monomers into dimers. The maximal concentration of EDOT<sub>2</sub> formed after one pulse is  $1.1 \times 10^{-5}\text{ mol L}^{-1}$ . This amount is much lower than that of EDOT molecules which remain in solution. As a consequence, if hydroxyl radicals react on both EDOT and EDOT<sub>2</sub> with the same rate constant, no competitive oxidation of EDOT<sub>2</sub> can be observed after only one pulse irradiation.

Let us suppose that such a step-by-step mechanism is correct; then if the dose per pulse deposited in the irradiated solution was much higher than 40 Gy or if a series of a very high number of successive pulses of 40 Gy was delivered in a concentrated volume of the irradiated solution, the concentration of hydroxyl radicals generated by radiolysis would be much higher and thus enough to oxidize EDOT into EDOT<sub>2</sub>, and also EDOT<sub>2</sub> and the successive oligomers into longer oligomers, inducing PEDOT growth.

**Electron Beam Irradiation. A Way for PEDOT Polymerization.** In our experiments the dose per pulse cannot be significantly increased. Then to check whether PEDOT polymerization effectively proceeds through a step-by-step oxidation process and with the aim to synthesize conducting PEDOT polymers by using an electron beam, we irradiated aqueous solutions containing 10 mM in EDOT in a closed cell under N<sub>2</sub>O atmosphere with a series of consecutive electron pulses of 40 Gy (delivered at a frequency of 10 Hz). In these conditions, a high concentration of oxidative species is produced. Note that in these experimental conditions, the electron accelerator was used as a simple high-energy electrons irradiator without any fast kinetic study.

Taking into account the step-by-step polymerization process described in the previous section, 10 mM hydroxyl radicals are needed for the quantitative dimerization of 10 mM EDOT into 5 mM EDOT<sub>2</sub>; then an additional amount of 5 mM HO<sup>•</sup> is needed for the quantitative transformation of EDOT into 2.5 mM EDOT<sub>4</sub> and so on. This means that at least 20 mM hydroxyl radicals is necessary to ensure the quantitative polymerization of EDOT monomers into PEDOT polymers. The use of two HO<sup>•</sup> radicals for one EDOT molecule is understandable since each EDOT monomer is bound to two EDOT neighbors inside the same polymer chain, which means that it has been twice oxidized. Thus, the theoretical irradiation dose ( $D_{\max}$ ) which should lead to the total oxidation of EDOT into PEDOT by HO<sup>•</sup> radicals can be calculated as follows:

$$D_{\max}(\text{Gy}) = \frac{2[\text{EDOT}]_0(\text{mol L}^{-1})}{G(\text{HO}^{\bullet})(\text{mol J}^{-1})} \quad (18)$$

where [EDOT]<sub>0</sub> corresponds to the initial concentration in EDOT in the aqueous irradiated solution.

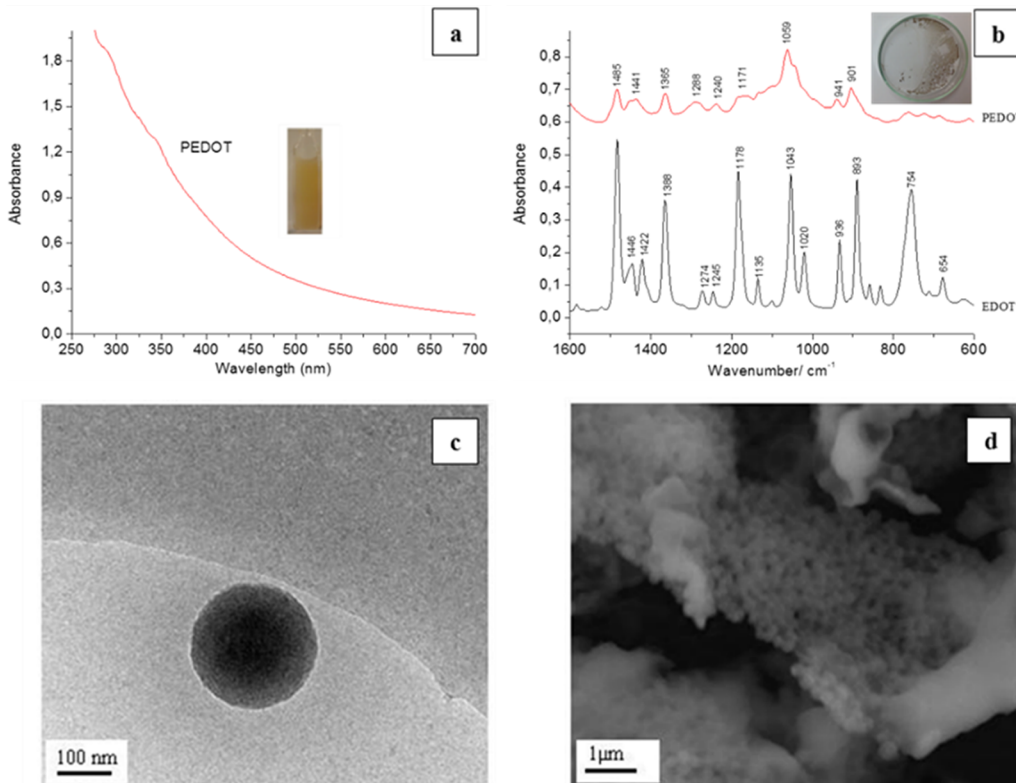


**Figure 7.** (a) Absorption spectrum of a  $\text{N}_2\text{O}$ -saturated aqueous solution of EDOT (10 mM) irradiated by an electron beam at a dose of 180 kGy (4500 pulses, 40 Gy/pulse). The reference was water, and path length was 1 mm; (inset) image of a cell containing PEDOT aqueous suspension radiosynthesized by an electron beam. (b) ATR-FTIR spectra of pure EDOT (bottom spectrum) and PEDOT polymers radiosynthesized at 180 kGy (top spectrum); (inset) photo of a cup containing the lyophilized radiosynthesized PEDOT powder. (c) Cryo-TEM image of radiosynthesized PEDOT in aqueous solution. A PEDOT nanoparticle of around 250 nm is observed. (d) SEM image of lyophilized radiosynthesized PEDOT powder. Aggregates of spherical PEDOT nanoparticles are observed.

According to eq 18, 37 kGy is necessary for the total polymerization of 10 mM EDOT. Knowing that each pulse corresponds to a dose of 40 Gy, complete polymerization requires more than about 1000 successive pulses.

To quantitatively polymerize EDOT, we irradiated the colorless and limpid aqueous solution of 10 mM EDOT at a dose of 180 kGy which corresponds to the accumulation of 4500 pulses at 40 Gy/pulse. After this irradiation, the solution became turbid. Figure 7a displays the UV-vis absorption spectrum. No noticeable absorption band is present in the spectrum. Nevertheless, a continuous scattering appears due to the presence of a brown-yellow suspension in the bulk of the irradiated solution (photo in inset of Figure 7a). This spectrum and the turbidity of the solution are in good agreement with the results we got in a previous work by  $\gamma$ -radiolysis,<sup>19</sup> suggesting that polymerization effectively took place.

To demonstrate that the radiosynthesized products are PEDOT polymers, the turbid solution obtained after 180 kGy electron beam irradiation was centrifuged to recuperate a solid phase. The isolated brown powder was lyophilized to eliminate any residual water molecules which could be trapped in the polymer-containing solid phase (photo in inset of Figure 7b). The solid sample was then characterized by ATR-FTIR spectroscopy to investigate the chemical nature of the obtained polymers.

The ATR-FTIR spectrum of the polymer powder is presented in the upper part of Figure 7b in the wavenumber region 1600–600  $\text{cm}^{-1}$  together with the spectrum of pure nonirradiated EDOT (bottom of Figure 7b). The two spectra are in good

agreement with those our group previously reported for PEDOT and EDOT when polymerization was induced by  $\gamma$ -rays (instead of accelerated electrons). The IR spectrum of the polymer powder displays vibrations at 1485, 1441, and 1365  $\text{cm}^{-1}$  which are attributable to C=C and C–C stretching modes in the thiophene ring. The vibrations observed at 1288, 1240, 1171, and 1059  $\text{cm}^{-1}$  are assigned to the stretching modes of the ethylenedioxy groups (C–C and C–O–R–O–C). The vibration modes of C–S bond which are present in the thiophene ring can be observed at 941 and 901  $\text{cm}^{-1}$ . Note that the intense C–H stretching band at 754  $\text{cm}^{-1}$ , observed in the spectrum of EDOT, is clearly absent in the ATR-FTIR spectrum of polymers. This definitely demonstrates, without any ambiguity, that EDOT polymerization quantitatively took place via  $\alpha,\alpha'$ -coupling reactions and that the resulting solid powder obtained after lyophilization is effectively composed of PEDOT polymers.

Our study demonstrates that instead of using  $\gamma$ -irradiation,<sup>20</sup> electron beam irradiation enables the radiosynthesis of PEDOT polymers. While one electron pulse leads to the formation of EDOT<sub>2</sub> dimers as stable products, the use of a series of successive pulses is necessary to generate enough hydroxyl radicals to form PEDOT polymers. We not only evidenced here that electron irradiation can be used as an alternative way for the synthesis of PEDOT polymers but also that PEDOT growth effectively proceeds through a step-by-step oxidation process as expected.

Aqueous solutions containing 10 mM in EDOT and irradiated by an electron beam at 180 kGy were observed by cryotransmission electron microscopy just after irradiation to investigate the structure and morphology of PEDOT polymers in

aqueous solution. Representative images show the presence of low density globular structures forming spherical nanoparticles with a diameter ranging between 200 and 250 nm as observed in Figure 7c. This result is in agreement with polymer size and shape found after  $\gamma$ -ray-induced PEDOT synthesis. Since no other low density objects were observed during our cryo-TEM experiments, we deduce that these spherical nanoparticles are made up of PEDOT polymers. Each observed nanoparticle should be composed of interdigitated polymer chains. Since no  $\alpha-\beta'$  linkages could occur during polymerization, radiosynthesized PEDOT nanostructures should be composed of linear chain polymers which are neither branched nor networked. Thus, the globular structure observed in Figure 7c should correspond to a self-assembly of independent amorphous PEDOT chain polymers. The presence of ethylenedioxy groups (H-bond acceptors) should explain not only the hydrosolubility of PEDOT polymers but also the as-observed packing and nanostructuration of the spherical supramolecular PEDOT self-assemblies.

To characterize the morphology of the polymers after a deposition procedure, the 180 kGy-irradiated sample was lyophilized and the black powder obtained was deposited and then characterized by SEM microscopy. The images indicate the presence of very close packed polymeric particles (Figure 7d). Once again PEDOT polymers appear as spherical nanoparticles. These structures should come from the globular nanostructures already observed in aqueous solution by cryo-TEM. The particles observed by SEM are almost monodisperse in size with a mean diameter of 220 nm which is close to that observed by cryo-TEM in aqueous solution. This proves that neither phase transition nor deposition procedure affects the size and shape of PEDOT nanoparticles. This would imply the existence of very strong hydrogen-bond interactions into each polymer nanoparticle.

We succeeded in the synthesis of PEDOT polymers by electron beam irradiation of EDOT aqueous solution. The radiosynthesized PEDOT polymers form monodisperse nanoparticles, the morphology of which is kept after deposition onto substrate. Since chemically and electrochemically synthesized PEDOT polymers are very often used for their conducting properties, we wanted to check by four-point probe technique whether our radiosynthesized PEDOT are also characterized by such interesting electrical properties.

After irradiation and lyophilization, the obtained PEDOT powder was dissolved and treated by a chemical oxidant  $\text{NOBF}_4$  ( $10^{-2}$  M) in acetonitrile. The solution was spin-coated onto a glass substrate, and a PEDOT layer was obtained. The average thickness of the doped PEDOT film was measured on a surface profiler and was found to be 105 nm. The mean value of the electrical conductivity was determined to be  $9 \times 10^{-4} \text{ S cm}^{-1}$ . This conductivity is comparable to the highest conductivities reported for PEDOT in the literature.<sup>55,56</sup> Nevertheless, we believe that the conductivity of radiosynthesized PEDOT could be further improved via control of the polymerization mechanism.

## CONCLUSION

Current research aims to develop new synthesis strategies and new conducting polymers with tuned morphologies and properties. We recently, and for the first time in the literature, used  $\gamma$ -radiolysis as an original simple alternative way for synthesizing nanostructured conducting polymers in solution. Nevertheless, the study of the influence of polymerization mechanism remains poorly investigated in the literature in the

field of conducting materials. We thus aimed to progress in this domain to better understand the growth process of conducting polymers and to find out a better way to optimize the preparation of nanostructured conducting polymers with adjusted morphologies and tuned properties.

In this work, a pulsed radiolysis study coupled with molecular simulations, with thermodynamic calculations, and with spectrokinetic analysis was used to study the mechanism of  $\text{HO}^\bullet$ -induced oxidation of EDOT in aqueous solution. The mechanistic scheme of EDOT oxidation by hydroxyl radical was established, the rate constants were determined, and the transient species involved in the oxidation process were identified via comparison of their experimental and simulated UV-vis absorption spectra. We used a mixed simulation method, using the Monte Carlo sampling of the molecular geometries, the DFT calculation of the electron structures, and the PCM modeling of the solvent. We had to tackle the spin contamination issue for open shell radicals. Nevertheless, we fixed it using an elementary spin screening procedure, inspired by the spin analysis of the TDDFT spectra and the spectrum of the quartet states. This procedure dropped spurious bands from the TDDFT spectra of the radical species and enabled a fruitful confrontation to the absorption spectra deduced from the experiments.

In acidic and neutral aqueous solutions,  $\text{HO}^\bullet$ -induced oxidation of EDOT implies the oxidation of EDOT into a transient species, namely  $\text{EDOT}^{+*}$  cation radical, which dimerizes and deprotonates, leading to a stable product, namely  $\text{EDOT}_2$  dimer. In alkaline medium, the mechanism is mostly different since  $\text{HO}^\bullet$  deprotonates into its alkaline form, oxide radical, which adds onto EDOT monomer. This addition leads to an open cycle and prevents any dimerization of EDOT and consequently any polymerization of PEDOT.

In acidic and neutral aqueous solutions, after one pulse irradiation (40 Gy), no products other than  $\text{EDOT}_2$  dimers were observed, demonstrating that no polymerization takes place. This proves that PEDOT polymerization is not a chain reaction. On the contrary, it proceeds through a step-by-step mechanism made up of the following recurrent steps: (i) oxidation/activation, (ii) growth/chain length increase, (iii) deprotonation. The amount of hydroxyl radicals generated by one pulse during the pulsed radiolysis study is then not enough to ensure polymerization. It only enables the incomplete transformation of EDOT monomers into dimers. The quantitative polymerization of EDOT into PEDOT requires a very much higher concentration in hydroxyl radicals which should reach at least twice that of EDOT.

To prove that PEDOT polymerization effectively proceeds through a step-by-step oxidation process and with the aim to synthesize conducting PEDOT polymers, we used the electron beam, usually employed in fast kinetic studies, as a high energy electron irradiator. Successfully, irradiation of EDOT aqueous solution with a series of 4500 consecutive electron pulses (180 kGy total dose) enabled the production of a very high concentration in hydroxyl radicals and thus the quantitative synthesis of PEDOT polymers, demonstrating that PEDOT growth proceeds through a step-by-step oxidation process as expected.

The chemical nature of radiosynthesized PEDOT polymers was confirmed by ATR-FTIR spectroscopy while their morphology was checked in solution by cryo-TEM microscopy and after lyophilization and deposition by SEM microscopy. Radiosynthesized PEDOT polymers were found to form monodisperse nanoparticles whose morphology was kept after

deposition onto solid substrate. Finally, the electrical conductivity of radiosynthesized PEDOT was evaluated at  $9 \times 10^{-4}$  S cm<sup>-1</sup>. This conductivity is comparable to conductivities already reported in the literature concerning PEDOT polymers synthesized by conventional methods.

These results encourage us to investigate the polymerization of other conducting polymers, such as polypyrrole, by using electron beam irradiation and to study the influence of the nature of alternative oxidizing radiolytic species onto the growth mechanism of conducting polymers. Also, we aim to synthesize conducting polymers directly onto a solid substrate and to follow the kinetic growth of the polymer films by using pulsed radiolysis.

To our best knowledge, this paper constitutes the first attempt in the literature to understand, through fast kinetics, the growth mechanism of conducting polymers. It also reports for the first time the use of an electron beam as an alternative way for the synthesis of conducting polymers. The present study bears witness to the tremendous potential of such a new electron-based methodology and gives us a glimpse of future promising industrial applications in the field of conducting polymers synthesis. Indeed, through accelerated electron-based nanobeams which are nowadays available, it should appear possible to synthesize conducting polymers onto conducting or even nonconducting substrates with a high spatial resolution to produce conductive patterns at a nanometric scale. The fact that conducting polymer growth proceeds through a step-by-step mechanism, and not according to a chain reaction, should enable the control of the chain length by adjustment of the irradiation dose.

## AUTHOR INFORMATION

### Corresponding Author

\*E-mail: samy.remita@u-psud.fr.

### Notes

The authors declare no competing financial interest.

## ACKNOWLEDGMENTS

We thank Jean-Philippe Larbre, Pierre Jeunesse, Audrey Gayral, Fabrice Gobert, and Alexandre Demarque for their assistance in the pulsed radiolysis experiments. We thank Mireille Benoit for helpful technical assistance in the chemistry laboratory. Also, we thank Fabrice Goubard and Pierre-Henri Aubert (LPPI, Université Cergy-Pontoise, France) for conductivity measurements, Jean-Michel Guigner (IMPMC, Université Pierre et Marie Curie, France) for Cryo-TEM experiments, and Patrice Lefrançois (PIMM, ENSAM/CNAM, France) for SEM observations. All the calculations were performed on the computing cluster of the Laboratoire de Chimie Physique. We thank Jean-Marie Teuler for his technical assistance.

## REFERENCES

- (1) Roncali, J.; Blanchard, P.; Frere, P. 3,4-Ethylenedioxothiophene (EDOT) as a Versatile Building Block for Advanced Functional  $\pi$ -Conjugated Systems. *J. Mater. Chem.* **2005**, *15*, 1589–1610.
- (2) Elschner, A. K. S.; Lo, W. *PEDOT Principles and Applications of an Intrinsically Conductive Polymer*; CRC Press: Boca Raton, FL, 2011.
- (3) Wang, Y. Research Progress on a Novel Conductive Polymer—Poly(3,4-Ethylenedioxothiophene) (PEDOT). *J. Phys. Conf. Ser.* **2009**, *152*, 012023.
- (4) Kvarnström, C.; Neugebauer, H.; Blomquist, S.; Ahonen, H. J.; Kankare, J.; Ivasaka, A. In Situ Spectroelectrochemical Characterization of Poly(3,4-ethylenedioxothiophene). *Electrochim. Acta* **1999**, *44*, 2739–2750.
- (5) Pei, Q.; Zuccarello, G.; Ahlskogt, M.; Inganäs, O. Electrochromic and Highly Stable Poly(3,4-Ethylenedioxothiophene) Switches between Opaque Blue-Black and Transparent Sky Blue. *Polymer* **1994**, *35*, 1347–1351.
- (6) Ha, Y.-H.; Nikolov, N.; Pollack, S. K.; Mastrangelo, J.; Martin, B. D.; Shashidhar, R. Towards a Transparent, Highly Conductive Poly(3,4-ethylenedioxothiophene). *Adv. Funct. Mater.* **2004**, *14*, 615–622.
- (7) Jin, Y.; Chen, Q. P.; Lessner, P. Thermal Stability Investigation of PEDOT Films from Chemical Oxidation and Prepolymerized Dispersion. *Electrochemistry* **2013**, *81*, 801–803.
- (8) Winther-Jensen, B.; Keld, W. Stability of Highly Conductive Poly(3,4-ethylene-dioxothiophene). *React. Funct. Polym.* **2006**, *66*, 479–483.
- (9) Cao, Y.; Yu, G.; Zhang, C.; Menon, R.; Heeger, A. J. Polymer Light-Emitting Diodes with Polyethylene Dioxythiophene–Polystyrene Sulphonate as the Transparent Anode. *Synth. Met.* **1997**, *87*, 171–174.
- (10) Roncali, J.; Frère, P.; Blanchard, P.; De Bettignies, R.; Turbiez, M.; Roquet, S.; Leriche, P.; Nicolas, Y. Molecular and Supramolecular Engineering of  $\Pi$ -Conjugated Systems for Photovoltaic Conversion. *Thin Solid Films* **2006**, *511–512*, 567–575.
- (11) Lee, S. J.; Pil Kim, H.; Mohd Yusoff, A. R. B.; Jang, J. Organic Photovoltaic with PEDOT:PSS and V<sub>2</sub>O<sub>5</sub> Mixture as Hole Transport Layer. *Sol. Energy Mater. Sol. Cells* **2014**, *120*, 238–243.
- (12) Yan, H.; Kagata, T.; Okuzaki, H. Micrometer-Scaled OFET Channel Patterns Fabricated by Using PEDOT/PSS Microfibers. *Synth. Met.* **2009**, *159*, 2229–2232.
- (13) Paradee, N.; Sirivat, A. Synthesis of Poly(3,4-ethylenedioxothiophene) Nanoparticles via Chemical Oxidation Polymerization. *Polym. Int.* **2014**, *63*, 106–113.
- (14) Chen, J. H.; Dai, C.-A.; Chiu, W.-Y. Synthesis of Highly Conductive EDOT Copolymer Films via Oxidative Chemical In Situ Polymerization. *J. Polym. Sci., Part A: Polym. Chem.* **2008**, *46*, 1662–1673.
- (15) Tamburri, E.; Orlanducci, S.; Toschi, F.; Terranova, M. L.; Passeri, D. Growth Mechanisms, Morphology, and Electroactivity of PEDOT Layers Produced by Electrochemical Routes in Aqueous Medium. *Synth. Met.* **2009**, *159*, 406–414.
- (16) Akoudad, S.; Roncali, J. Electrochemical Synthesis of Poly(3,4-ethylenedioxothiophene) from a Dimer Precursor. *Synth. Met.* **1998**, *93*, 111–114.
- (17) Sakmeche, N.; Aeiyach, S.; Aaron, J. J.; Jouini, M.; Lacroix, J. C.; Lacaze, P. C. Improvement of the Electrosynthesis and Physicochemical Properties of Poly(3,4-ethylenedioxothiophene) Using a Sodium Dodecyl Sulfate Micellar Aqueous Medium. *Langmuir* **1999**, *15*, 2566–2574.
- (18) Rocha, I.; Lucht, E.; Riegel-Vidotti, I. C.; Vidotti, M.; Orth, E. S. Kinetic Approach to Elucidate Size Controllable Features in Nano-composites of Gold Nanoparticles and Poly(3,4-ethylenedioxothiophene) in Aqueous Dispersion Stabilized by Gum Acacia. *J. Phys. Chem. C* **2014**, *118*, 25756–25764.
- (19) Lattach, Y.; Deniset-Besseau, A.; Guigner, J.-M.; Remita, S. Radiation Chemistry as an Alternative Way for the Synthesis of PEDOT Conducting Polymers under “Soft” Conditions. *Radiat. Phys. Chem.* **2013**, *82*, 44–53.
- (20) Lattach, Y.; Coletta, C.; Ghosh, S.; Remita, S. Radiation-Induced Synthesis of Nanostructured Conjugated Polymers in Aqueous Solution: Fundamental Effect of Oxidizing Species. *ChemPhysChem* **2014**, *15* (1), 208–218.
- (21) Belloni, J.; et al. ELYSE—A Picosecond Electron Accelerator for Pulse Radiolysis Research. *Nucl. Instrum. Methods A* **2005**, *539*, 527–539.
- (22) Marignier, J. L.; De Waele, V.; Monard, H.; Gobert, F.; Larbre, J. P.; Demarque, A.; Mostafavi, M.; Belloni, J. Time-Resolved Spectroscopy at the Picosecond Laser-Triggered Electron Accelerator ELYSE. *Radiat. Phys. Chem.* **2006**, *75*, 1024–1033.
- (23) Ferradini, C.; Jay-Gerin, J. P. The Effect of pH on Water Radiolysis: A Still Open Question - A Minireview. *Res. Chem. Intermed.* **2000**, *26*, 549–565.

- (24) Buxton, G. V.; Greenstock, C. L.; Helman, W. P.; Ross, A. B. Critical-Review of Rate Constants for Reactions of Hydrated Electrons, Hydrogen-Atoms and Hydroxyl Radicals ( $\text{OH}^{\cdot}/\text{O}^{\bullet-}$ ) In Aqueous-Solution. *J. Phys. Chem. Ref. Data* **1988**, *17*, 513–886.
- (25) Rabani, J. L. W. A. J. The Pulse Radiolysis of Dearthed Aqueous Carbonate Solutions I. Transient Optical Spectrum and Mechanism II. pK for OH Radicals. *J. Phys. Chem.* **1966**, *70*, 2100–2106.
- (26) Ruckebusch, C.; Sliwa, M.; Pernot, P.; De Juan, A.; Tauler, R. Comprehensive Data Analysis of Femtosecond Transient Absorption Spectra: A Review. *J. Photochem. Photobiol. C* **2012**, *13*, 1–27.
- (27) R Core Team. *R: A Language and Environment for Statistical Computing*; R Foundation for Statistical Computing: Vienna, Austria, 2014.
- (28) M.Mullen, K. ALS: Multivariate Curve Resolution Alternating Least Squares (MCR-ALS). R Package Version 0.0.5, 2012.
- (29) Ghalanos, A.; Theussl, S. Rsolnp: General Non-Linear Optimization Using Augmented Lagrange Multiplier Method. R Package Version 1.14, 2012.
- (30) Ma, J.; Archirel, P.; Schmidhammer, U.; Teuler, J. M.; Pernot, P.; Mostafavi, M. Reduction of Earth Alkaline Salts in THF Solution Studied by Picosecond Pulse Radiolysis. *J. Phys. Chem. A* **2013**, *117*, 14048–14055.
- (31) Becke, A. D. Density Functional Thermochemistry. III The Role of Exact Exchange. *J. Chem. Phys.* **1993**, *98*, 5648–5652.
- (32) Dunning, T. H., Jr. Gaussian Basis Sets for Use in Correlated Molecular Calculations: The Atoms Boron through Neon and Hydrogen. *J. Chem. Phys.* **1989**, *90*, 1007–1023.
- (33) Fuentealba, P.; Preuss, H.; Stoll, H.; V. Szentpaly, L. A Proper Account of Core-Polarization with Pseudopotentials: Single Valence Electron Alkali Compounds. *Chem. Phys. Lett.* **1989**, *89*, 418–422.
- (34) Ungerer, P.; Tavitian, B.; Boutin, A. Applications of Molecular Simulation in the Oil and Gas Industry. *Monte-Carlo Methods*; Editions Technip: Paris, 2005.
- (35) Frisch, M. J. et al. *Gaussian 09, Revision D.01*; Gaussian, Inc., Wallingford, CT, 2013.
- (36) Marenich, A. V.; Cramer, C. J.; Truhlar, D. J. Universal Solvation Model Based on Solute Electron Density and a Continuum Model of the Solvent Defined by the Bulk Dielectric Constant and Atomic Surface Tensions. *J. Phys. Chem. B* **2009**, *113*, 6378–6396.
- (37) Lever, A. B. P.; Gorelsky, S. I. Ruthenium Complexes of Non-Innocent Ligands: Aspects of Charge-Transfer Spectroscopy. *Struct. Bonding (Berlin)* **2004**, *107*, 77–114.
- (38) Saunders, B. B.; Kaufman, P. C.; Matheson, M. S. Reactions of Thiophene with Radiolytically Produced Radicals. 1. The Hydroxyl Radical. *J. Phys. Chem.* **1978**, *82*, 142–150.
- (39) Saunders, B. B. Reactions of Thiophene with Radiolytically Produced Radicals. 2. The Solvated Electron and the Hydrogen Atom. 2. *J. Phys. Chem.* **1978**, *82*, 151–154.
- (40) Gaikwad, P.; Priyadarshini, K. I.; Naumov, S.; Rao, B. S. Oxidation of Tryptamine and 5-Hydroxytryptamine: A Pulse Radiolysis and Quantum Chemical Study. *J. Phys. Chem. A* **2009**, *113*, 8249–57.
- (41) Singh, T. A.; Rao, B. S. M.; O'Neill, P. Radical Chemistry of 8-Oxo-7,8-dihydro-2'-deoxyadenosine and 8-Oxo-7,8-dihydro-2'-deoxyguanosine: a Pulse Radiolysis Study. *J. Phys. Chem. B* **2010**, *114*, 16611–16617.
- (42) Dorfman, L. M.; Adams, G. E. Reactivity of the Hydroxyl Radical in Aqueous Solutions. *National Standards Reference Data System*, National Bureau of Standards, 1973
- (43) Kirchmeyer, S.; Reuter, K. Scientific Importance, Properties and Growing Applications of Poly(3,4-ethylenedioxothiophene). *J. Mater. Chem.* **2005**, *15*, 2077–2088.
- (44) Vasantha, V. S.; Phani, K. L. N. Effect of Hydroxypropyl-beta-cyclodextrin on the Electrochemical Oxidation and Polymerization of 3,4-Ethylenedioxothiophene. *J. Electroanal. Chem.* **2002**, *520*, 79–88.
- (45) Rezać, Ž. Cuby 4, Software Framework for Computational Chemistry.
- (46) Rabilloud, F.; Harb, M.; Ndome, H.; Archirel, P. UV-visible Absorption Spectra of Small Platinum Carbonyl Complexes and Particles. A Density Functional Theory. *J. Phys. Chem. A* **2010**, *114*, 6451–6462.
- (47) Hirschfelder, J. O. Hyperviriel Theorem for Classical and Quantum Mechanics. *J. Chem. Phys.* **1960**, *33*, 1462–1466.
- (48) Xu, J.; Xu, H.; Quan, J. C.; Sha, F.; Yao, C. 2-Chloromethyl-2,3-dihydrothieno-[3,4-b]dioxine. *Acta Crystallogr., Sect. E: Struct. Rep. Online* **2009** *E65*, o668.
- (49) Fukuda, R.; Nakatsuji, H. Formulation and Implementation of Direct Algorithm for the Symmetry-Adapted Cluster and Symmetry-Adapted Cluster-Configuration Interaction Method. *J. Chem. Phys.* **2008**, *128*, 094105.
- (50) Lattach, Y.; Archirel, P.; Remita, S. Influence of the Chemical Functionalities of a Molecularly Imprinted Conducting Polymer on its Sensing Properties: Electrochemical Measurements and Semiempirical DFT Calculations. *J. Phys. Chem. B* **2012**, *116*, 1467–1481.
- (51) Born, M. *Z. Phys.* **1920**, *1*, 45–48.
- (52) Tissandier, M. D.; Cowen, K. A.; Feng, W. Y.; Gundlach, E.; Cohen, M. H.; Earhart, A. D.; Coe, J. V.; Tuttle, T. R., Jr. The Proton's Absolute Aqueous Enthalpy and Gibbs Free Energy of Solvation from Cluster-Ion Solvation Data. *J. Phys. Chem. A* **1998**, *102*, 7787–7794.
- (53) Ahonen, H. J.; Lukkari, J.; Heellström, T.; Mattila, J.; Kankare, J. Characterisation of Poly(3,4-ethylenedioxothiophene) films polymerised in aqueous media. *Synth. Met.* **2001**, *119*, 119–120.
- (54) Neta, P. S. H. Rate Constants for the Reaction of Oxygen( $\cdot$ ) Radicals with Organic Substrates in Aqueous Solution. *J. Phys. Chem.* **1975**, *79*, 1–6.
- (55) Jones, B. H.; Cheng, K. Y.; Holmes, R. J.; Lodge, T. P. Nanoporous Poly(3,4-ethylenedioxothiophene) Derived from Polymeric Bicontinuous Microemulsion Templates. *Macromolecules* **2012**, *45*, 599–601.
- (56) Ghosh, S.; Remita, H.; Ramos, L.; Dazzi, A.; Deniset-Besseau, A.; Beaunier, P.; Goubard, F.; Aubert, P. H.; Brisset, F.; Remita, S. PEDOT nanostructures synthesized in hexagonal mesophases. *New J. Chem.* **2014**, *38*, 1106–1115.